

MADIS UMALAS

Application of sol-gel technology
for production of ceramic
nanocomposites and functional coatings



MADIS UMALAS

Application of sol-gel technology
for production of ceramic
nanocomposites and functional coatings



Institute of Physics, Faculty of Science and Technology, University of Tartu,
Estonia

Department of Materials Engineering, Faculty of Mechanical Engineering,
Tallinn University of Technology.

The dissertation was admitted on March 18, 2015 in partial fulfilment of the requirements of the degree of Doctor of Philosophy in Material Science and allowed for defence by Scientific Council on Material Science of Faculty of Science and Technology, University of Tartu, Estonia.

Supervisors: Dr. Ants Lõhmus, Institute of Physics, University of Tartu
Dr. Rünno Lõhmus, Institute of Physics, University of Tartu
Dr. Irina Hussainova, Department of Materials Engineering,
Tallinn University of Technology

Opponents: Dr. Karin Mougín, Institut de Science des Matériaux de
Mulhouse
Dr. Valdek Mikli, Keemia ja materjalitehnoloogia
teaduskond, Tallinna Tehnikaülikool,

Commencement: June 5, 2015 at University of Tartu, Tartu, Estonia.

This work has been partially supported by graduate school “Functional materials and technologies” receiving funding from the European Social Fund under project 1.2.0401.09-0079 in Estonia; Estonian Nanotechnology Competence Centre.



European Union
European Social Fund



Investing in your future

ISSN 2228-0928
ISBN 978-9949-32-798-0 (print)
ISBN 978-9949-32-799-7 (pdf)

Copyright: Madis Umalas, 2015

University of Tartu Press
www.tyk.ee

CONTENTS

LIST OF ORIGINAL PUBLICATIONS	6
ABBREVIATIONS AND SYMBOLS	8
PREFACE	9
1. LITERATURE OVERVIEW	12
1.1. Carbide matrix composites	12
1.1.1. Transition metal carbides	12
1.1.2. TiC-ZrC compounds	14
1.1.3. Synthesis methods of TiC, ZrC and TiC-ZrC	16
1.1.4. Sintering of TiC, ZrC and TiC-ZrC.....	17
1.2. Ceramic matrix CNT and fibres composites	19
1.3. Functional multisystem ceramic coatings.....	20
1.4. Mechanical characterization of reinforcement agent.....	22
1.5. Sol – gel method.....	25
1.5.1. Introduction of sol-gel method	25
1.5.2. Synthesis of transition metal oxide by sol-gel.....	26
1.5.3. Synthesis of metal carbides precursor by sol-gel method	28
1.5.4. Heat treatment of synthesised gel precursor.....	29
2. AIM OF THESIS	31
3. MATERIALS AND METHODS	32
3.1. Synthesis of TiC-ZrC and TiC/MWCNT (papers I, II, V, VII).....	32
3.2. Synthesis of titania coatings on AgNWs network (paper IV)	34
3.3. Annealing of alumina nanofibers and AgNW sample preparation for mechanical characterisation (papers III, V).....	35
3.4. Sample characterization.....	35
3.5. Mechanical characterization of individual 1D nanostructures (papers: III, VI).....	36
3.5.1. Development of experimental set-up	37
4. RESULTS AND DISCUSSIONS	40
4.1. Synthesis of TiC – ZrC composite (papers I, II, V).....	40
4.2. Synthesis of TiC/MWCNT composites powders	46
4.3. Mechanical characterization of annealed Al ₂ O ₃ nanofibers (paper VI) .	50
4.4. Preparation of titania and Ag NW random network functional coatings by sol – gel method (papers III, IV)	53
CONCLUSION	59
SUMMARY IN ESTONIAN	61
ACKNOWLEDGEMENTS	63
REFERENCES	64
PUBLICATIONS	75
CURRICULUM VITAE	132
ELULOOKIRJELDUS.....	134

LIST OF ORIGINAL PUBLICATIONS

- I. **M. Umalas**, V. Reedo, A. Lõhmus, and I. Hussainova, (2012). „Sol – gel solution based processing for nanocarbides. In: Proceedings of the 8th International Conference of DAAAM Baltic Industrial Engineering 19–21st April 2012, Tallinn, Estonia: 8th International Conference of DAAAM Baltic Industrial Engineering, Tallinn, Estonia, 19–21 april 2012. (Toim.) Otto, Tallinn: Tallinna Tehnikaülikooli Kirjastus, 2012, 753 – 758
- II. **M. Umalas**, V. Reedo, A. Lõhmus, I. Hussainova, and K. Juhani, “Synthesis of ZrC-TiC Blend by Novel Combination of Sol-Gel Method and Carbothermal Reduction,” *Key Eng. Mater.*, vol. 527, pp. 62–67, Nov. 2012.
- III. S. Vlassov, B. Polyakov, L. M. Dorogin, M. Antsov, M. Mets, **M. Umalas**, R. Saar, R. Lõhmus, and I. Kink, “Elasticity and yield strength of pentagonal silver nanowires: In situ bending tests,” *Mater. Chem. Phys.*, vol. 143, no. 3, pp. 1026–1031, Feb. 2014.
- IV. **M. Umalas**, S. Vlassov, B. Polyakov, L. M. Dorogin, R. Saar, I. Kink, R. Lõhmus, A. Lõhmus, and A. E. Romanov, “Electron beam induced growth of silver nanowhiskers,” *J. Cryst. Growth*, vol. 410, pp. 63–68, Jan. 2015.
- V. **M. Umalas**, I. Hussainova, V. Reedo, D.-L. Young, E. Cura, S.-P. Hannula, R. Lõhmus, and A. Lõhmus, “Combined sol–gel and carbothermal synthesis of ZrC–TiC powders for composites,” *Mater. Chem. Phys.*, vol. 153, pp. 301–306, Mar. 2015.
- VI. M. Vahtrus, **M. Umalas**, B. Polyakov, L. Dorogin, R. Saar, M. Tamme, K. Saal, R. Lõhmus, S. Vlassov, “Mechanical and structural characterization of gamma and alpha alumina nanofibers” *Materials Characterization* (submitted)

Other papers in related field:

- VII. Invention: Method for synthesiz of stabilized oxide nanomateric size particles in ionic liquids Owner: University of Tartu and Estonian Nanotechnology Competence Centre; Authors R. Välbe, R. Lõhmus, M. Tarkanovskaja, U. Mäorg, V. Reedo, **M. Umalas**, J. Kübarsepp, A. Lõhmus. IT/N31274, 18.06.2014

Author's contribution

- Paper I, II, V:** The author is responsible for synthesis of TiC-ZrC powders by combination of sol-gel and carbothermal reduction and for composing the manuscript. The author carried out XRD, Raman, SEM characterisation and data processing.
- Paper III:** The author participated in development of experimental equipment and carrying out the experiments.
- Paper IV:** The author is responsible for the preparation of manuscript and preparing the samples using sol-gel method. The author participated in SEM characterization and revealing of silver nanowhiskers growth. The author is responsible of XRD, Raman measurements and interpretation.
- Paper VI:** The author is responsible for sample preparation and XRD characterization. The author participated in development of experimental equipment and carrying out the experiments related to the sample treatment. The author participated in manuscript preparation.

ABBREVIATIONS AND SYMBOLS

acac	Acetylacetone
ADC-DAC card	Analog-to-digital converter card
AFM	Atomic force microscopy
AgNW	Silver nanowires
CMC	Ceramic matrix composites
CNTs	Carbon nanotubes
fcc	Face-centered cubic crystal lattice
HRSEM	High resolution scanning electron microscopy
Hy	benzene-1,4-diol
IR	Infrared
ITO	Indium tin oxide
MeC	Metal carbide
MeO	Metal oxide
MWCNT	Multiwall carbon nanotubes
NEMS	Nanoelectromechanical system
NW	Nanowires
PVP	Polyvinylpyrrolidone
QTF	Quartz tuning fork
SEM	Scanning electron microscopy
SHS	Self-propagating high-temperature synthesis
SPF	Superplastic forming
SPS	Spark plasma sintering
STM	Scanning tunneling microscope
TEM	Transmission electron microscopy
UHTCs	Ultra high temperature ceramics
UHV	Ultra high vacuum
UV	Ultraviolet
XRD	X-ray diffraction

PREFACE

The conventional industry is undergoing a dramatic change towards an innovative, high-tech, knowledge-based grounds. Increasing competition on the global market constantly demands for materials with advanced properties and producing technology. Advanced microscopy and characterization technologies at the nanoscale may help not only to understand, but also to design and control the properties of nanomaterials. [1]

The most common way to design materials with advanced properties is to combine two or more known materials with desired characteristics into one structure. One widespread approach of combining different materials is to mix them together making so called “composite material” where one or more phases of one material (filler or reinforcement agent) dispersed in another (matrix) material. As a result enhanced mechanical properties, increased thermal and electrical conductivity, reduction of the overall production costs, etc. can be achieved [2].

One of the most common types of composite materials is ceramic matrix composites (CMCs). CMCs have been developed to overcome intrinsic brittleness and mechanical unreliability of monolithic ceramics, which are otherwise attractive for their high stiffness and strength. In addition to mechanical effects, the reinforcing agent may contribute to other properties such as electric conductivity, thermal expansion coefficient, hardness and thermal shock resistance [3], [4]. On the other hand the ceramic matrix could protect filler components from corrosion and act as a thermal and electrical insulator [5], [6].

Another way of combining two different materials is to coat one structure with thin layer of another, whereas at least one of them can be multi-component (composite). Multi-component coatings have become important in developing coatings with functional properties and are widely demanded by hi-tech industry in key applications such as protective, antireflection, flexible and transparent electrodes, antibacterial coatings and sensors [7][8]. The combination of these properties makes CMCs and multi component ceramic coatings very attractive functional and structural materials for a variety of applications.

To overcome intrinsic brittleness of CMC materials and multi component ceramic coatings the reinforcing agent should be tougher than the matrix. Size and shape of the filler particles are also of great importance in making composite materials and multi-component coatings. Depending on applications filler particles may have various geometries from spherical to long fibres and even layers, but the size in most cases is restricted to nanoscale at least in one spatial direction. Micro- and macro particles can also give certain benefits, however they act as a stress concentrators, causing decrease in strain to failure, strength and toughness. Moreover, macroscopic materials themselves have many defects and dislocations that severely compromise their mechanical performance. Nanostructures, in contrast, have little or no defects over their entire extent resulting in exceptional mechanical and other properties. [9]

Typical examples of materials used as nanofillers are e.g. ceramic nanofibers, nanowires and carbon nanotubes (CNT). This naturally leads to conclusion, that development of nanocomposites and nanostructured coatings are more relevant and preferable research directions in modern material science.

The particular aim of this thesis is related to elaboration of ceramic nanocomposites and functional coatings with desired properties by sol-gel method. Sol-gel is chosen since in contrast to conventional ceramic materials synthesis methods, in sol-gel process reactants are mixed together at molecular level due to the synthesis conditions enabling to decrease synthesis temperatures and prepare homogeneous and pure multi component systems. In particular, the thesis describes the synthesis of TiC-ZrC, TiC/CNT and AgNW/TiO₂ nanocomposites precursors. The problems of dispersion and thermal stability of filler material are treated. Moreover, the thesis reports mechanical characterisation of individual nanofillers like Al₂O₃ nanofibers and AgNW using advanced experimental set-up installed inside a scanning electron microscope. Development and construction of experimental equipment are also involved. For convenience, synergy between different topics of the thesis is schematically shown in figure below.

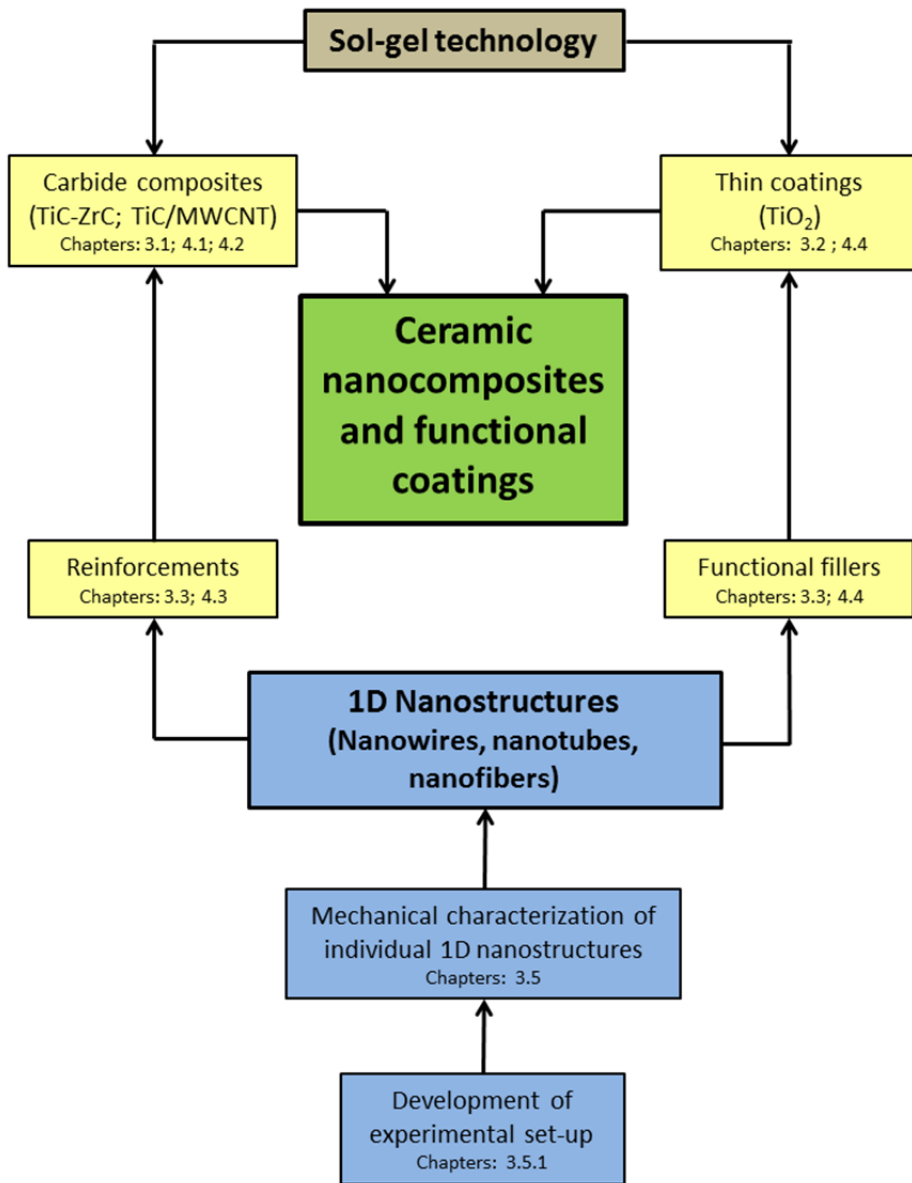


Figure A. Schema of connection between the thesis topics

I. LITERATURE OVERVIEW

I.1. Carbide matrix composites

During recent decades researchers have paid great attention to new materials that are stable at extreme environmental conditions as candidates for technological applications like supersonic flight and rocket propulsion. Ultra High Temperature Ceramics (UHTCs), based on carbides, nitrides, and borides of some transition metals have received a lot of attention in this field. These materials are promising candidates for thermal protection system due to their excellent and unique combination of high melting point, good thermal-shock resistance and high hardness [10]. Brittleness and poor oxidation resistance of carbides make them unreliable for usage in important construction details. In order to overcome the restrictive properties the development has moved in direction of multicomponent carbides (carbide matrix composites). Recent research shows that carbon fibres, carbon nanotubes (CNTs) and other carbide or refractory metals reinforced carbide matrix composites can prevent inherent brittleness [11] [12] [13]. Elaboration of carbide matrix composites with functional properties like low thermal expansion coefficient, desired tribological performance and energy efficient synthesis methods is of increasing importance for new commercial applications like brake disks and pads, clutches, calibration plates or furnace charging devices [14].

I.1.1. Transition metal carbides

Carbides are a compound of carbon and other elements with a smaller or the same electronegativity. Carbides that are formed by transition metals of IVB group (titanium zirconium and hafnium) are called IVB group metal carbides. These carbides are sometimes referred as refractory carbides, which means that the carbides have a melting point greater than 1800 °C and a high degree of chemical stability [15]. The refractory properties of carbides are caused by strong metal-to-carbon and metal-to-metal bonds [16]. In this research project of TiC, ZrC and their compounds (TiC-ZrC) were in focus of the investigation. Titanium carbide (TiC) and zirconium carbide (ZrC) have same face centered cubic (f c c) crystal structure and have similar properties and characteristics [16]. In the (f c c) crystal structure the titanium and zirconium atoms are situated in a face-centered cubic close-packed arrangement with the octahedral interstitial sites being occupied by carbon atoms (Figure 1) [17].

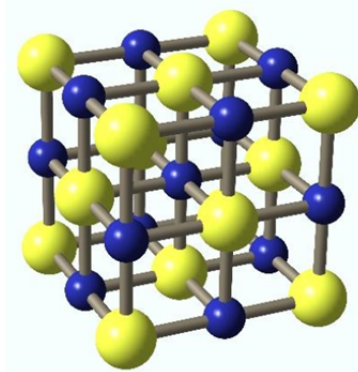


Figure 1. Face centered cubic crystal structure of TiC and ZrC. Blue ball stands for carbon atom and yellow one is for a metal atom

These carbides have extreme hardness, strength and high melting points. They are brittle, which make titanium and zirconium carbides typical ceramic materials [18]. Physical and mechanical properties of these carbides are summarised in Table 1 and 2. It must be noted that there is some variation of carbide properties in the literature. These variations can be caused by non-stoichiometries in tested phases; the purity of tested phases is sometimes unclear. The values given in Table 1. stand for composition of the closest to the exact stoichiometry. Titanium and zirconium oxides are insulators but the corresponding carbides have lower electrical resistivity and belong to semiconductors [19]. In addition to high melting points of TiC and ZrC, they have high thermal stability and good chemical resistance. TiC is resistant to most acids, for except of HNO₃ and HF that can attack it. ZrC is not as chemically resistant as TiC, since cold HNO₃ and cold mixture of H₂SO₄ and H₃PO₄. can dissolve it. Both TiC and ZrC can be heated in inert environment to their melting point without decomposing [15].

Table 1. Structural, physical and thermal properties of TiC and ZrC [15]

Compound	Lattice structure	Lattice parameter (Å)	Density (g/cm ³)	Melting point (°C)	Thermal conductivity at 20 °C (W/m-K)	Thermal expansion at 20 °C (x10 ⁻⁶ /°C)	Electrical resistivity at 20 °C (μΩ · cm)
TiC	cubic	4.328	4.90	3067	21.0	7.4	68
ZrC	cubic	4.698	6.59	3420	20.5	6.7	43

Due to their specific properties carbides are important materials for industry. Carbides are traditionally used as cutting tools, abrasives, wear and corrosion applications [15][16][20]. During the last decade, transition metal carbides and composites have found use in new promising fields such as electrode materials

for low temperature fuel cells [21]. The catalytic properties of transition metal carbides are similar to those of noble metals (Pt, Pd, Rh and Ru) for some chemical and electrochemical reactions, including oxidation of hydrogen, CO, alcohols, and reduction of oxygen. Transition metal carbides like TiC have also metallic electrical conductivity and good microwave absorption with a minimum reflection loss which makes them suitable for use as counter-electrodes in dye sensitized solar cells [22] and electromagnetic wave absorption [23]. ZrC has been considered for nuclear fuel applications because attractive properties for ZrC as a nuclear fuel material include high melting point above 3500 K (for near-stoichiometric compositions), generally good resistance to fission products attack, high thermal conductivity at very high temperatures, and low neutron absorption cross-section [24].

1.1.2. TiC-ZrC compounds

Low fracture toughness of single transition metal carbides is a limiting factor for its applications [19], [25] [26]. To overcome the low fracture toughness of carbides, refractory metals like molybdenum as a binder metal [13];[27] and/or toughening compounds such as tetragonal zirconia ($t\text{-ZrO}_2$) that undergo phase transformation from its tetragonal polymorph into monoclinic one, are added [28], [29]. Mixed carbides have been also considered as attractive materials due to their enhanced properties originated from the complementary effects of each single metal carbide [21]. Moreover two phase compounds with fine grain size could exhibit “superplasticity”. [30]

Superplasticity refers to an ability of polycrystalline solids to exhibit exceptionally large elongation under tension. Superplasticity commonly explained as grain boundary sliding at elevated temperatures. The essential mechanism of superplasticity is the accommodation process of grain boundary sliding so that the polycrystalline materials can be stretched extensively without fracture. The application of superplasticity makes it possible to fabricate ceramic components by superplastic forming (SPF).[31]

Theoretical calculations have shown that TiC and ZrC with similar cubic crystal structure can form binary compounds and solid solutions with different properties than that of single phase materials. It is theoretically expected that the physical and mechanical properties of TiC-ZrC compound could be altered by varying the TiC and ZrC concentrations in the compound. [32]. The different ionic radii of Ti and Zr atoms make it difficult to obtain a completely solid solution at a wide range of composition and temperatures. To obtain solid solution high sintering temperatures and suitable concentration of TiC and ZrC are required [33].

The mechanical properties of TiC, ZrC, and $\text{Ti}_x\text{Zr}_{x-1}\text{C}$ solid solutions and binary compound are summarised in Table 2. to compare the changes in mechanical properties. In Table 2 some properties of TiC-ZrC compounds are not shown because these compounds are not yet studied so precisely. Recent

research [25] has demonstrated that TiC can be used as a reinforcing agent to improve fracture toughness and reduce the sintering temperature of ZrC. The highest fracture toughness $6.3 \text{ MPa} \cdot \text{m}^{1/2}$ was achieved for binary compound composition of $\text{TiC}_{0.3}\text{-ZrC}_{0.7}$ (mole concentrations). Another research group [34] has presented a solid solution with similar concentration $\text{TiC}_{0.3}\text{-ZrC}_{0.7}$ (mole concentrations) having similar fracture toughness $6.2 \text{ MPa} \cdot \text{m}^{1/2}$ compared to the binary compound.

Table 2. Mechanical properties and sintering methods of TiC, ZrC and their compounds

Compod	Number of phases	Young's modulus (GPa)	Vickers hardness (HV1) (GPa)	Fracture toughness ($\text{MPa} \cdot \text{m}^{1/2}$)	Sintering properties	Reference
TiC	one phase	410–510	28–35	3.6–3.8	–	[15],[16]
ZrC	one phase	350–440	29.9	3	–	[15],[16]
$\text{TiC}_{0.7}\text{-ZrC}_{0.3}$	two phase	360	24	5.5	Spark plasma sintering at $1800 \text{ }^\circ\text{C}$, pressure 50 MPa, for 5 min	[34]
$\text{TiC}_{0.5}\text{-ZrC}_{0.5}$	two phase	390	22.5	5.5		
$\text{TiC}_{0.3}\text{-ZrC}_{0.7}$	one phase	395	20	6.2		
$\text{TiC}_{0.7}\text{-ZrC}_{0.3}$	two phase		21.7	5.26	Hot pressed at $1900 \text{ }^\circ\text{C}$ and 21MPa, for 1 hour	[35]
$\text{TiC}_{0.5}\text{-ZrC}_{0.5}$	two phase		22.2	5.19		
$\text{TiC}_{0.3}\text{-ZrC}_{0.7}$	two phase		21.8	5.27		
$\text{TiC}_{0.24}\text{-ZrC}_{0.76}$	one phase		22.1	3.54	Spark plasma sintering between $1750\text{--}1850 \text{ }^\circ\text{C}$ for 300 s, uniaxial pressure of 40 MPa	[19]
$\text{TiC}_{0.63}\text{-ZrC}_{0.37}$	two phase		21.5	5.8	Mechanically pressed at 20 Mpa and sinterd at $1900 \text{ }^\circ\text{C}$ fo r 30 m	[25]
$\text{TiC}_{0.5}\text{-ZrC}_{0.5}$	two phase		23.6	5.0		
$\text{TiC}_{0.3}\text{-ZrC}_{0.7}$	two phase		20.4	6.3		

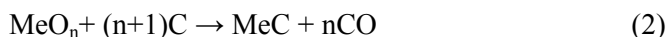
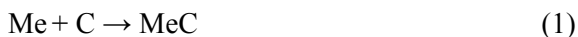
The summary table of mechanical properties shows increasing of fracture toughness of TiC-ZrC solid solutions and binary compound at all range of compositions and sintering methods comparing to pure TiC and ZrC. The fracture toughness increase can be explained by grain boundary pinning by the intergranular structure [34]. Varying concentrations of TiC and ZrC do not demonstrate considerable changes in mechanical properties. Correspondingly structural and composition analysis of these compounds has shown that in case of titanium concentration of 0.3–0.7 two phase compounds are achieved and close to the end of phase diagram ZrC and TiC single phase solid (TiZrC₂) solutions are formed.

The production of these materials as solid solutions or binary compound may lead to ability to tailor the nanostructure of these materials to further improvement of mechanical properties. The studies showed that these compounds may offer an alternative way to improve mechanical properties without additional fibres, CNTs or whiskers.

1.1.3. Synthesis methods of TiC, ZrC and TiC-ZrC

Unlike oxides which can be produced from raw materials found in the nature, the refractory carbides generally do not exist in the natural state. The synthesis of refractory carbides is costly and time consuming because these materials are high stability, chemical inertness and a general tendency to decompose upon melting [15]. Various synthesis methods enable producing refractory carbides, like nano-, micro-powders by carbothermal reduction [36] [37], sol-gel [18] [38] and self-propagating high-temperature synthesis [39]; dense bodies by sintering, pressure sintering and spark plasma sintering [40], [41],[42]; fibres/whisker by sol-gel [43][44][45], coatings by chemical-vapour deposition (CVD) [46] [47], physical-vapour deposition (PVD) [48] [49] and thermal spray [50].

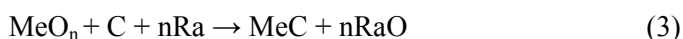
In this section let us out synthesis methods that are commonly used to synthesis TiC, ZrC and their compounds powders. The most common methods to synthesis transition-metal carbides (TiC, ZrC) powders are reaction of metal (Me = Ti, Zr) or metal oxide (MeO_x = TiO₂, ZrO₂) and carbon (C) in the form of powders and in inert or reducing atmosphere (Equation 1 and 2.). These reactions take place in the temperature range of 1500 °C to 2400 °C and the reaction times can range from 10 to 24 h, depending on the metal [15] [36].



To get fine size and stoichiometric carbide powders it is necessary to mill primary powders before annealing. Another method to synthesize the carbides is high-energy milling of metal oxide with graphite which reduces crystallite size to achieve almost amorphous powders exhibiting quite low transition

temperature around 1300–1500 °C [25], [51]. The previous methods are energy and time consuming and a final product suffers from impurities and is inhomogeneous because the powders are mixed together on a relatively coarse scale (e.g., micro-scale) and attrition of milling media increase concentration of the impurities [52].

Self-propagating high-temperature synthesis (SHS) is widely used technology to synthesize refractory carbides. In this method, the chemical and phase compositions of the synthesis products can be easily controlled and are low energy and time consuming [53]. In the process of SHS the reaction takes place with metal oxide (TiO₂ or ZrO₂) and carbon. In order to activate this reaction it is necessary to add a reducing agent (Ra = Mg) [39] (Equation 3). These reactants interact in two stages: firstly the reduction of parent metal oxide and secondly interaction of the reduced metal with carbon to form the refractory carbide [54]. Result of self-propagating high-temperature synthesis is an intermediate product including metal carbide and an oxide of reducing metal. The oxide of reducing metal is uniformly distributed over the reaction product. Further treatment of the synthesis product by acid-washing is needed to remove oxide of reducing metal and to get pure carbide powder.[39]



The sol-gel process is very flexible, it is a suitable method to synthesize a wide variety of ceramic materials, most commonly is used in synthesis of metal oxide but it is also a suitable method for metal carbides and nitrides [18][55][56]. Titanium and zirconium polymeric precursors are prepared from metalorganic compounds, usually titanium and zirconium alkoxides and additional reactant for increasing carbon concentration in the polymer precursor [57][58]. During the pyrolysis and carbothermal reduction carbide polymeric precursors can be easily converted into carbide [59]. In the metal carbide polymeric precursors reactants are homogeneously distributed at molecular level. That reduces the kinetic barriers between the developed metal oxide and the carbon particles created in pyrolysis of a metal alkoxide polymer precursor. The increased contact area of the nanograins results in carbothermal reduction between the metal oxide and carbon particles at lower temperature and shorter time as compared to conventional carbide synthesis methods. Moreover, the use of molecular precursors and the control of the synthesis conditions are described in section 1.5.3.

1.1.4. Sintering of TiC, ZrC and TiC-ZrC

Due to the high melting point of refractory carbides it is necessary to use heat treatment to convert carbide powders into a dense solid. The compacted products of refractory carbides are produced by powder metallurgy technology where firstly powder is pressed to the required shape and then sintered at high temperatures (1900–2700 °C) [15], [40]. Required shape green bodies are

heated to a temperature that is 0.5 – 0.9 of melting point and atomic diffusion in the solid facilitates joining of the powder particles and reducing of porosity [60]. A small amount (2–10%) of binder agent such as cobalt, nickel and molybdenum are added to carbide powders to reduce sintering temperature [27], [61]. This method is referred to as liquid-phase sintering where binder agent wets carbide particles and fill pores at sintering temperature. For efficient and rapid liquid-phase the carbide phase should be at least slightly soluble in the liquid phase to enhance liquid atomic diffusion and mass transport [62].

In some case previous sintering methods do not give desired density and mechanical properties are not so suitable for applications [13]. To get higher density and fine grain size can be achieved by adding external pressure during sintering. This method is referred to as a pressure sintering [60]. For refractory carbides is most commonly used a hot pressing which is one of the pressure sintering method. During sintering of TiC and ZrC carbide at temperature of 2000 °C the powders are pressed at 30 MPa to get a dense body [63] [64].

For the densification of refractory carbides one can use also spark plasma sintering method (SPS). SPS is an effective technique for preparing dense refractory carbides and other ceramics materials. During SPS, the rapid and thorough heat distribution along the specimen generated from the high-frequency transformation and dispersion of the spark. Joule heat makes it possible to densify the materials at a low temperature (around 1800 °C) and in a short time [41] [42].

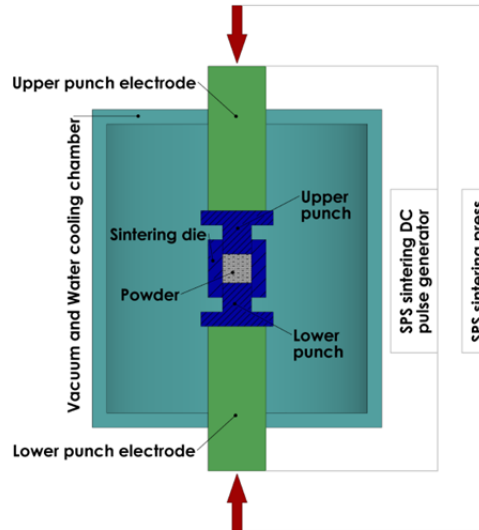


Figure 2. Scheme of spark plasma sintering setup [65]

1.2. Ceramic matrix CNT and fibres composites

Ceramic matrix composites (CMCs) have been developed to overcome ceramic material brittleness and to tune other mechanical properties. In addition to mechanical properties, the reinforcing phase may alter more properties such as electrical conductivity, thermal expansion, hardness and thermal shock resistance [66].

Wide range of reinforcing agents has been considered for designing ceramic materials with unique and desired properties. In particular, carbon nanotubes (CNTs) and oxide fibre have been considered to improve fracture toughness of ceramics [67],[68]. The key issue to produce CNTs and fibre based composites is distribution of reinforcing agent in matrix material. The individual nanotube or fibre should be distributed uniformly throughout the matrix and well-separated from each other. The presence of agglomerates can act as defects leading to stress concentration and premature failures. CNTs and fibres tend to agglomerate into bundles by van der Waals forces due to their relatively high surface areas and their high aspect ratios [66]. Another important aspect is strong interfacial bonding of the reinforcing agents with the host matrix components to have an efficient load transfer from host matrix to reinforcing agents. By achieving that, it is possible to obtain high performance materials with multi-functional properties [69].

The surface of reinforcing agent is often modified, either by direct functionalization or by the use of surfactants, in order to add stability in a given solvent or to improve compatibility with a given matrix. Commonly for activation of CNTs surface is realized in harsh conditions such as chemical oxidation by strong acids such as HNO_3 , H_2SO_4 and KMnO_4 . Chemical oxidation is an effective way to increase the solubility and chemical reactivity but such treatment can cause defects on the CNT surface structure which leads to reduction of mechanical and electrical properties [70]. In order to avoid damaging of CNT surface it is good to use polymeric surfactants like polyvinylpyrrolidone (PVP) or PMMA[71]. Q. Y. Tang et al. demonstrated that use of the PVP as surfactant gives stable dispersion of CNTs for two months [72].

If the reinforcing agent dispersion is sufficient then it will be mixed with a conventional ceramic powder, a colloidal ceramic suspension or sol-gel precursor to obtain composite. Up to now, sol-gel method has been widely used to fabricate CNT/ceramic composites because it makes possible to create intimate dispersion of the CNTs in inorganic matrices, as well as a good adhesion of the host matrix to CNT, when a proper surfactant is used. The advantages of sol-gel for conventional powders processing are that ball milling is not necessary to mixing CNTs in ceramic matrix. Ball milling could damage CNTs, and shorter CNTs could be a less efficient reinforcement or induce an undesirable effect on physical properties of CNTs ceramic matrix composites [66] [67] [73].

Inbaraj et al. [74] has prepared high purity alumina and MWCNT composites by an aqueous sol-gel processing route with a hardness of 2150 ± 20 (Kg/mm^2)

and a fracture toughness of $5.5 \pm 0.2 \text{ MPa m}^{1/2}$. C. Zhang et al. [75] showed a possibility to use polymeric glue between SWCNT and sol of titania, alumina and silicon to fabrication ceramic oxide-coated SWNT composites by sol-gel method.

Fracture toughness of ceramics can also be increased with use of metal oxide nanofibres as reinforcement. B.N. Dudkin et al. [76] described synthesis of corundum matrix ceramic composite reinforced with surface modified alumina nanofibres. The mechanical characterization showed that alumina nanofibers have positive effect on the strength and fracture toughness of the matrix. The bending strength of the composite reinforced with modified alumina nanofibres was twice that of the composite reinforced with unmodified nanofibres.

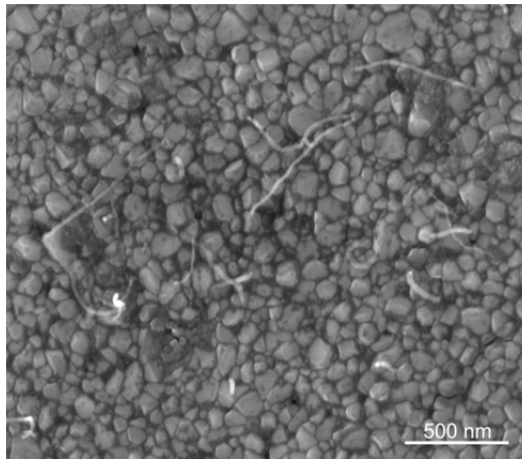


Figure 3. Illustrative images of Al₂O₃-0.35%wt CNT composite

I.3. Functional multisystem ceramic coatings

Development of nanostructured ceramic coatings has become an important research area mainly due to the interesting chemical and physical properties of nanoscale materials. Nanostructured coatings with enhanced functional and mechanical properties are demanded in high-tech industry in key applications such as protective, antireflection, medicine, flexible and transparent electrodes, and antibacterial coatings [7][8].

Generally, scratch resistant nanostructured ceramic coatings are used to protect a soft plastic or metal substrate from abrasion [77]. In order to ensure maximal protection, coatings should have good corrosion and wear resistance, low friction and high value of hardness. In addition coating should rub against other surfaces without a liquid lubricant. So they should be self-lubricating to guarantee long life time of protection [78]. The self-lubricating coatings are very attractive for biological and space applications. D. M. Martinez et al. [79]

have studied Ti-Zr-C-H coatings as potential candidates for protective layers for biocompatible applications. The constituting elements were selected due to their proven good biocompatibility at the macroscale. It was proposed that Ti-Zr-C coating is surrounded with soft hydrogenated amorphous carbon matrix which reduces hardness and elastic modulus. Moreover, these films exhibit low friction coefficients due to the amorphous matrix with lubricating properties.

It is well known that structural factors can affect significant functional properties of coatings, including the size, specific surface area, pore volume, pore structure, crystalline phase, and the exposed surface facets. For example TiO₂ nanoparticles can be used for the photocatalytic effect [80], [81] UV-absorbing properties [82], and anatase TiO₂ coatings for biocide properties [83], and silver nanowires (AgNW) as transparent conducting material [84].

Under UV irradiation the TiO₂ polycrystalline coatings become highly hydrophilic and highly oleophilic. Such highly amphiphilic surfaces could be used in windows antifogging and self-cleaning applications. In addition to the amphiphilic surfaces R. Wang et al. [80] demonstrated that ultraviolet irradiation from sunlight is sufficient to maintain the amphiphilic surface, so that hydrophilic or oleophilic contaminants on the surfaces can easily removed by rain.

An effective method to enhance titania photocatalytic and other properties is to dope it with anions or cations. Metal doping like cobalt has long been known to be one of the most effective ways to change the electronic band structure of TiO₂, and consequently, to improve its visible light sensitivity as well as increase its photocatalytic activity under UV irradiation. Among other dopants, Ag has got much attention for this purpose [85], [86]. O. Akhavan [86] has showed Ag doped TiO₂ thin coatings have excellent photocatalysis, long lasting antibacterial properties and appropriate for biomedical and antibacterial applications.

One of the main applications for functional multisystem ceramic coatings is flexible and transparent electrodes. Contacting metal oxide coatings such as aluminium dope zinc oxide and indium tin oxide (ITO) have found a use as transparent conductors in touch screens, solar cells and organic light emitting diodes.[87] Nowadays researches have focused on searching for alternative material for ITO which is mostly used as transparent electrode. The brittle nature of the ITO coatings makes its use difficult on flexible substrates and sputtering process of ITO would damages organic optoelectronic device. Recently AgNWs have been attracted interest as a transparent conducting material based on random AgNW network. It is a promising material for transparent electrode because it can lower network resistance ($\sim 9.7\Omega/\text{sq}$) and can have high transmittance ($\sim 89\%$ at 550 nm). The latter is defined as the fraction of light able to pass through the open spaces between the nanowire network [84], [88]. The AgNWs also have outstanding elastic properties which is making it promising materials for flexible transparent electrodes. S. Vlassov et. al [89] have demonstrated that AgNWs have high fatigue resistance and can be bent elastically multiple times to significant curvatures without failure. A. Kim

et. al [84] have developed ZnO/AgNW/ZnO composite electrode which demonstrated good thermal and mechanical stabilities as well as a high conductivity and good transparency. Cu(In,Ga)(S,Se)₂ (CIGSSe) thin film solar cells incorporating this composite electrode exhibited a 20% increase of the power conversion efficiency compared to a conventional sputtered indium tin oxide-based CIGSSe solar cell.

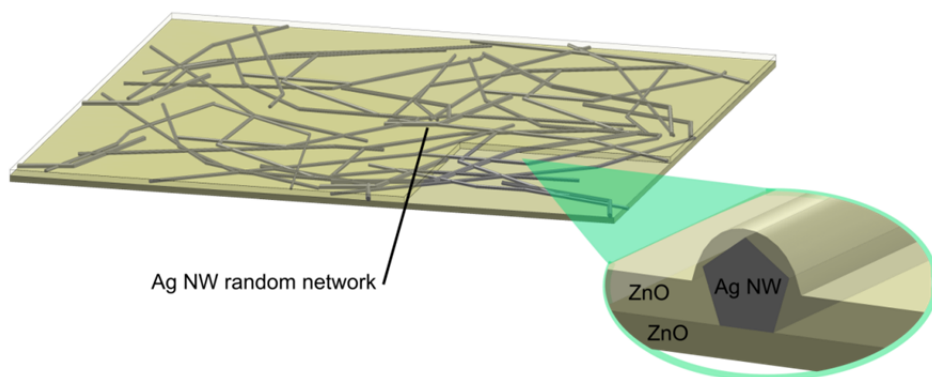


Figure 4. Illustrative scheme of ZnO/Ag nanowire/ZnO composite electrode for thin film solar cells [84]

Although these excellent properties of AgNWs it has some drawbacks for replacement of ITO based electrodes. The AgNW can be exposed to air and temperature approximately at 200 °C. The AgNWs network would suffer from local oxidation and melting which affects the conductivity of the network. Coating of AgNWs network with thin oxide layer could potentially protect them from the corrosion [90]. Moreover, it was recently demonstrated that TiO₂ shells increase thermal stability of individual AgNWs [6].

In this work protection of random AgNW network by thin TiO₂ coatings is discussed. One of the widely used methods for preparing TiO₂ coatings is sol-gel processing which make possible to design desired structural, electrical and photocatalytical properties. The sol-gel process for synthesis of TiO₂ is described in details in section 1.5.

I.4. Mechanical characterization of reinforcement agent

In order to successfully utilize the advantages of nanofillers and to maximize the overall effect on properties of nanocomposite or nanocoating, it is important to carefully choose the appropriate filler material. Therefore, studies of individual nanostructures via fine nanoscale experiments made with top-level

modern scientific equipment [91], [92] are necessary for deeper understanding of dependence of the nanostructure properties on composition, structure, size, geometry and conditions. Knowledge gained in nanoscale experiments will give ability to tune the properties of the nanostructures at production and synthesis stage to meet the particular needs of the final composite product. Methods employed for mechanical characterization of CNT, nanofibre's, fibres and whiskers, typically include nanoindentation, three point bending test or tensile test.[9] [93]

Common tool used for mechanical testing and manipulation of individual nanostructures is atomic force microscopes (AFM) due to high force resolution. Z. Zhao et al. [94] and P. Zhang et al.[95] were measured the elastic modulus of a single alumina nanofiber using the three-point bending method by contact mode AFM. Both research groups have shown that elastic modulus of nanofibers is much lower than of the commercial alumina fibres which is beneficial when they are subjected to mechanical contact stress during their service lifetime. E. Wong et al. [96] were measured elastic properties and mechanical strength of SiC nanorods and MWCNT deposited on low friction substrate (MoS_2) using AFM lateral force regime. The MWCNTs were about two times as stiff as the SiC nanorods. Continued bending of the SiC nanorods ultimately led to fracture, whereas the MWCNTs exhibited an interesting elastic buckling process.

AFM methods have certain limitations. AFM can be used either for visualisation or for measurements, but not both at the same time. It means, that first image of the investigated object should be taken, then measurement is performed, and the image is taken again to see the results of the measurements. Therefore, a measurement with AFM is time-consuming and there is no real-time visual feedback concerning the behaviour of the investigated object during testing. It means that information on crack formation and propagation, changes in diameter etc is absent. Only indirect conclusions can be drawn on the basis of the shape of the force curves. Additionally, typically AFM experiments are made in ambient conditions, meaning that a considerable amount of water is present on all surfaces under investigation, complicating the interpretation of forces [97].

To overcome above-mentioned problem measurement set-up should be installed inside electron microscope. Such configuration provides direct real-time observation of the dynamic events as they are progressing and qualitative information about the mechanism of the motion and deformation. Technically in situ experiments can be realized by installing piezo positioners and scanners equipped with a sharp probe into electron microscope. E.g. Zhu et al. [98] performed in situ tensile tests of AgNWs inside SEM. NW were fixed between the nanomanipulator tip and AFM cantilever and then pulled until failure. Young's modulus, yield strength, and ultimate strength were calculated from the deflection of the AFM cantilever with known spring constant. The measurements shows that young's modulus, yield strength, and ultimate tensile strength all increased as the NW diameter decreased.

Nanomechanical testing can also be carried out by a nanoindenter inside SEM. This kind of set-up has been applied to measure the nanomechanical load frames performed by micro-cantilever beam experiments on bio-inspired composites [99]. The FIB micro-milling setup was used to cut out the rectangular micro-cantilever beam from bulk composite. An indenter equipped with a 5- μm radius 60-degree conospherical diamond indenter probe was used for mechanical characterisation of cantilever beam. This research provided evidence that the oriented nanoclay tablets embedded in the polymer matrix of the nanocomposite deflect the trajectory of propagating cracks and the tensile stress in the cantilever beam reached 430 MPa.

It is also important to point out, that different measurement techniques may give different values of mechanical characteristics. The effect of the different measurement techniques on the measured values of the Young's modulus were demonstrated by Rohlig et al. [100] for ZnO NWs and Polyakov et al. [92] for SiO₂ NTs by comparing bending test, three point bending test, tensile and compressive strain. The differences up to approximately 40% were demonstrated. These investigations point out that for better understanding of material's behaviour under different loading conditions important for the particular applications it is necessary to use different measurement techniques to get information about certain properties.

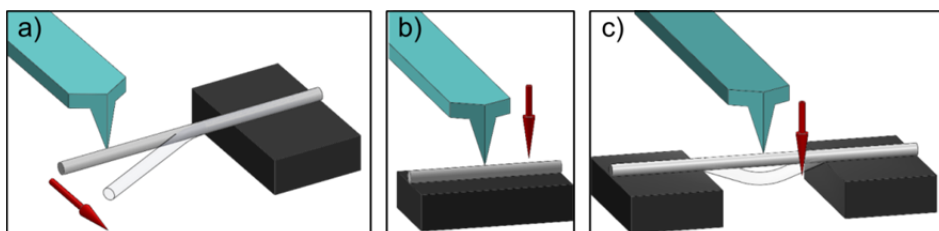


Figure 5. Schematics of different variations of mechanical testing of 1D nanostructures a) beam bending b) nanoindentation and c) three point beam bending.

In spite of obvious advantages in situ SEM experiments have certain limitations and peculiarities that should be taken into account. Electron beam (e-beam) irradiation can cause significant charging of poorly conducting materials that may influence the interaction between investigated object and the tip. Moreover radiation defects can occur and affect the determination of mechanical properties. Zheng et al. [101] have shown a moderately intense electron beam (10^{-2} A/cm²) in transmission electron microscope (TEM) causing radiation defects in silica NWs which can be induced enabling significant superplastic elongations $> 200\%$ in tensile tests. They also report the quantitative comparison of the load-displacement responses without and with the e-beam, revealing dramatic difference in the flow stress. Vlassov et al [5] demonstrated electron beam induced viscoelasticity and shape restoration effect in Ag/SiO₂ core-shell nanowires. One more e-beam related problem is assisted carbon

deposition. High energy electrons can decompose hydrocarbons molecules, which are present in the vacuum chamber and amorphous carbon can be deposited on the areas exposed to electron beam for prolonged periods. Amount of deposited carbon depends on the vacuum level, e-beam energy, the presence of hydrocarbon inside the chamber and exposition time. [102]

Another limitation that should be taken into account when planning an experiment inside SEM is associated with the resolution of electron microscope. First, typical scanning rate of the electron beam is limited to a few Hz, therefore only relatively slow processes can be visualized. Resolution and signal intensity are reversely proportional to scanning speed. Visible dimensions of the nanostructures at magnification close to the resolution limit are sensitive to brightness/contrast settings of a microscope. It can be problematic to identify the exact shape of the NW cross section, for example, to distinguish between square and slightly rectangular cross sections or estimate degree of hexagon or pentagon distortions.[102]

I.5. Sol – gel method

I.5.1. Introduction of sol-gel method

Sol-gel technology is a versatile technology, making it possible to produce a wide variety of materials and to provide existing materials with novel properties. The sol-gel method is a widely used technique for producing metal oxide powders, aerogels, xerogels, films and fibres with controlled parameters [103] [104]. Particularly, the sol-gel process has become a very popular fabrication method in industries, according the American Ceramic Society market analysis the global market for sol-gel products reached \$1.4 billion in 2011 and it will further grow to \$2.2 billion by 2017 [105]. The sol-gel technology has received so much scientific and technological attention because it has many advantages compared to conventional powder processing methods. Lower temperatures are required for material processing. Homogeneous and pure multi-component systems can easily be obtained by mixing the molecular precursor solutions [106]. This technology provides the ability to control molecular-scale mixing and the ability to form the M1–O–M2 bonds (where M1 and M2 denote two different cations) to synthesis multi-component metal oxides and carbides [107], [108]. In some particular cases the sol-gel method could cause drawbacks which are connected to proceeding condition, most problematic issues are gel drying, aging, environment humidity and temperature. All these previous issues could affect reproducibility of products.

1.5.2. Synthesis of transition metal oxide by sol-gel

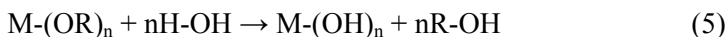
The most used molecular precursors are metal alkoxides which have high purity compared to mined raw materials. All metals form corresponding alkoxides and they have general formula 4:



where M is the metal and R is an alkyl group and x is the valence state of the material [109]. Metal alkoxides are very reactive toward nucleophilic reagents such as water. This high chemical reactivity is due to the low electronegativity of the metal and render metal atom susceptible to nucleophilic attack. The metal alkoxide should be handled with great care due to the high chemical reactivity of metal alkoxide with water. To avoid a spontaneous reaction between the metal alkoxide and water, the humidity should be controlled or stabilized by an acid or basic.[110]

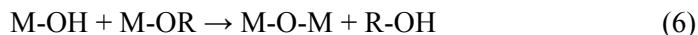
The present overview is focused on the synthesis of transition metal oxide thin films (e.g. titanium dioxide) by sol-gel process. The transition metal alkoxide are less durable to hydrolysis, condensation and other nucleophilic reactions than silicon alkoxides which are the most commonly used precursor in sol-gel processes. The lower electronegativity of transition metals causes them to be more electrophilic and have higher reactivity.[111]

The basic idea of the synthesis of metal oxides by sol-gel process is hydrolysis and polycondensation of metal alkoxides or other molecular precursors. Firstly the hydrolysis of metal alkoxide takes place and a reactive metal hydroxo group $M-(OH)_n$ is generated due to nucleophilic substitution of alkoxy groups by water (Eq. 5). The mechanism involves nucleophilic addition followed by proton transfer [104].

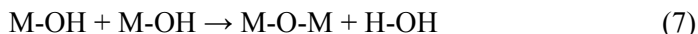


Polycondensation of metal alkoxides will start as soon as hydroxo groups are generated and depending on the chemical reaction condition, three competitive mechanisms have to be considered: alcoxolation, oxolation and ololation. During the polycondensation, hydrolysed precursor can react either with alkoxy precursor (alcoxolation Eq. 6) or with other hydrolysed precursors (oxolation Eq. 7). In addition, bridging hydroxo groups can be formed through the elimination of a solvent molecule, this kind of reactions is called ololation (Eq. 8, 9). This reaction occurs when the full coordination of the metal atom is not satisfied in the alkoxide. The latter can be either H_2O or $R-OH$ depending on the water concentration in the medium. In result of the three condensation mechanisms oligo- and polymeric chains $(-M-O-)_n$ are formed and this leads to the formation of a 3D network. The dominating condensation mechanism depends on the reaction conditions (pH, water/alkoxide ratio, temperature, concentration of metal alkoxide) and precursor alkoxides. [104] [110]

Alcoxolation



Oxolation



Olation



The hydrolysis and polycondensation mechanism are more detail described by J. Livage [110].

Hydrolysis and polycondensation of titanium alkoxides ($\text{Ti}(\text{OR})_4$) flows as described above. The hydrolysis of titanium alkoxides is fast, 90% of alkoxy groups are hydrolysed after 1000s and polycondensation starts immediately after approximately 25 to 50% of the alkoxy groups are hydrolysed [112]. The hydrolysis of titanium alkoxides starts with the protonation of a negatively charged alkoxide oxygen atom which results in releasing an alcohol molecule. The reaction times for titanium alkoxides hydrolysis are in the order of magnitude of milliseconds and in case of zirconium alkoxides microseconds [113]. The product of polycondensation of titanium alkoxides is never 100% titanium oxide, there are some amount of Ti-OH and Ti-OR groups. B. Yoldas [114] has shown in his research that the titanium oxide content varies from ~70% to over 90% pending of starting titanium alkoxides ($\text{Ti}(\text{OC}_2\text{H}_5)_4$, $\text{Ti}(\text{OC}_3\text{H}_7)_4$ and $\text{Ti}(\text{OC}_4\text{H}_9)_4$) and water concentration. In sol-gel process it is very important to control the hydrolysis of metal alkoxides and polycondensation to produce a homogeneous metal oxide network. Therefore it is essential to use chelating reagents such as diols, basics, acids or diketone compounds to modify the metal alkoxides. In most cases, the modification takes place following a proton-assisted $\text{S}_{\text{N}}1$ reaction mechanism [106], [113]. A.O Aroyinbo et al. [115] have reported that the grain size of TiO_2 increases from about 40 nm to 450 nm with increasing pH from acidic to base. It is due to the fact that an average Milliken charge of hydrogen atoms around the titanium coordinated complexes at low pH is much more than at high pH. The complexes will be separated well because of the repulsive force at low pH which results in a slow and discrete disposition of the complexes on the performed nuclei, which leads to forming small nanocrystallites. At higher pH values, the titanium coordinated complexes could not be separated well due to a smaller repulsive force and this results in a fast disposition, which leads to the grain size increase. V. Kessler et al. have deeply studied the chemical modification of metal alkoxides by carboxylic acids, β -diketones. In their research “New insight in the role of modifying ligands in the sol-gel processing of metal alkoxide precursors: A possibility to approach new classes of materials” [113] they have disproven

the former explanation of the modification of metal alkoxides with chelating ligands. Formerly the chemical modification of metal alkoxides with different chelating ligands is explained as follows: the chelating ligands not changing significantly the charge distribution in the molecules but they are blocking the coordination sites of the metal atoms, and shielding the metal atoms from polycondensation by non-hydrolysable and thus not removable ligands. V. Kessler et al. have explained it differently: The whole process of sol formation is thus directed not by kinetics of hydrolysis and polycondensation, but by the self-assembly of ligands. The modifying ligands are forming the particles of sols through their interaction with the solvents and can stabilize dispersions in essentially the same way as surfactants. The formed hydrated oxides are hydrophilic, which means that the polar solvents are favouring the direct and non-polar ones-inverted micellar self-assembly. The chemical modification does not lead to decreased rate of hydrolysis and polycondensation reactions, however, it does really result in slowing down or even preventing the gelation and, especially, the uncontrolled precipitation on addition of water.

During a gelation process the formation of 3D-network of sol particles will occur. The gelation process begins with interaction of the particles in sol with each other and forms clusters which aggregate until 3D-network, also called gel, is formed. The interaction can occur either via hydrogen bonding or via coalescence with formation of M–O–M bridges [116]. The aggregation of particles can take place in two ways. At smaller hydrolysis ratios or/and in the presence of chelating ligands strongly interacting with the solvent, the primary particles form aggregates that have a possibility to develop common surface with strong interaction towards the solvent. At high hydrolysis ratios and in the absence of heteroligands, the particles aggregate through the volume of the solvent forming dense gels or precipitates [116] [117].

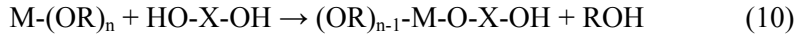
The 3D-network can be dried in various conditions leading to forming a xerogel with residual porosity. During drying the solvent is removed from the pores and due to the capillary pressure increase the network shrinks. After drying the xerogel volume was reduced compared to the volume of the wet network [118]. Further heating of the xerogel in controlled conditions allows obtaining the desired metal oxides phases. The desired phases are usually lower than the ones required by solid-state processes. [119].

1.5.3. Synthesis of metal carbides precursor by sol-gel method

The sol–gel process has been examined as a cost-effective alternative for classically used powder processing methods to synthesise metal carbides to reduce the carbothermal reaction temperature. The sol-gel process is used for the synthesis of metal carbide precursor materials before carbothermal reduction. As for the synthesis of metal oxides by sol-gel, the metal carbide precursor is prepared according to the metal alkoxide polycondensation mechanism

which goes through a gelling stage followed by drying and consolidation. [15] [106]

To synthesise metal carbide precursor gel by sol-gel method the metal alkoxide polycondensation is carried out by a transesterification of the OR groups in metal alkoxide $M-(OR)_n$ by adding ligands which act as bridging ligands. Usually diols or other chemicals are used as bridging ligands which having two or more reactive OH groups [120], [121]. The transesterification (Eq. 10) followed by polycondensation (Eq. 11) of $M-(OR)_n$ is showed in sequent equation:



The transesterification process is necessary to increase the carbon content of carbon in precursor gel for carbothermal reduction to synthesise stoichiometry metal carbides.[57] The carbon content of the precursor gel depends on the bridging ligands, H. Press et al. [59] have studied the different bridging ligands like diols, dihydroxybenzenes, dihydroxycarboxylic acids and saccharose as bridging ligands for synthesising TiC and ZrC. The use of different bridging ligands results in polycondensation yielding either spinnable viscous solutions or elastic gels and for stoichiometric carbon content it is suitable use dihydroxybenzenes or saccharose as bridging ligands. Sometimes the secondary carbon sources (bridging ligands) adding in metal carbide polymeric precursor is not needed. M.D. Sacks et al. [122] . have synthesised HfC using a single source precursor.

As described in previous section, polycondensation the synthesis of metal oxides by sol-gel method results in wet gel. This needs to be dried and further heated to reduce the xerogel precursor to metal carbide and metal oxide. The heat treatment for oxide gel precursor and carbide gel precursor is described in next section.

I.5.4. Heat treatment of synthesised gel precursor

Both the metal oxide and carbide xerogel precursors need to be heat treated in order to remove organic residues and transfer the metal oxides or carbides to desired crystalline phases.

For oxides this further heat treatment is called annealing. Majority of xerogels are amorphous and porous after drying. During annealing the surface energy decreases and the pores collapse. Viscous flow of the material results in a dense structure. Crystalline material annealing involves diffusion and is a slower process than viscous flow and needs higher temperatures. It is important to densify the xerogel at lower temperatures and then carry out the crystallization at higher temperatures. [118]

In case of titania xerogel precursors crystalline phase is achieved by sintering at relatively high temperatures in air. Anatase phase typically appears after thermal treatment at 400 °C and transits to rutile crystal phase at approximately 800 °C. [85] [123] [124]

The main difference between heat treatment of metal oxide and metal carbide precursors is that the metal carbide heat treatment is carried out in an inert atmosphere. To get pure metal oxides it is necessary to remove all organic residues from the precursor but in case of metal carbides it is important to convert organic residues to carbon. This needs to be done to reduce metal oxides to metal carbide. Heat treatment of metal carbide precursor xerogel can be divided in two parts: pyrolysis and carbothermal reduction. The xerogel precursors were heated up to 800 °C during the pyrolysis of TiC and ZrC and the precursor decomposes into rutile TiO₂, tetragonal ZrO₂ and amorphous carbon. [125], [126]. Carbothermal reduction of TiO₂, ZrO₂ and amorphous carbon to corresponding metal carbides starts when the Gibbs free energy becomes negative during heat treatment. C.R. Rambo et. al. [127] calculation shows that Gibbs free energy becomes negative for TiC at 1050 °C and for ZrC 1350 °C, at atmospheric pressure. V. G. Sevastyanov et al. [125] have shown that the reduction of carbon begins at lower temperatures, for TiC at 950 °C and ZrO₂ at 1050 °C, at pressure of 1×10^{-4} MPa. These results are in good agreement with the temperatures of the Gibbs free energy calculation at fixed pressure of 1×10^{-4} MPa. Previous discussion shows that the reaction temperature decreases with the system pressure decrease. MeC are easily formed in vacuum for CO can easily leave from the material. Therefore, the reduction of MeC in vacuum is easier than at atmospheric pressure. [37], [52]

2. AIM OF THESIS

Goal of the work described in the thesis was elaboration of ceramic-matrix composites and functional coatings with desired properties by combining advantages of sol-gel technique and nanostructured fillers. To achieve this goal a number of tasks were assigned, which include issues of synthesis, processing and characterization of the materials under investigation. All activities are interconnected and reinforce each other.

The main objectives are listed below:

- Synthesis of TiC-ZrC composites by combination of sol-gel method and process of carbothermal reduction, and mechanical characterization of the composites produced.
- Development and characterization of TiC/MWCNT composites by sol-gel method and carbothermal reduction.
- Benchmark applicability of commercially available (*MemPro Ceramics*) alumina nanofibers as a promising reinforcement material in CMCs.
- Benchmark applicability of AgNWs for flexible composite coatings.

3. MATERIALS AND METHODS

3.1. Synthesis of TiC-ZrC and TiC/MWCNT (papers I, II, V, VII)

In the present work the combination of sol-gel and carbothermal reduction methods was used to elaborate the method of synthesis of TiC-ZrC and TiC/MWCNT composite powders. Sol-gel method was used to synthesize polymeric xerogel precursors of TiC-ZrC and TiC/MWCNT composite. The xerogel precursors were prepared from commercially available chemicals: titanium (IV) n-butoxide, $\text{Ti}(\text{OC}_4\text{H}_9)_4$, (99+%, Alfa-Aesar or Sigma-Aldrich, reagent grade), zirconium (IV) n-butoxid, $\text{Zr}(\text{OC}_4\text{H}_9)_4$, (80%, in butanol, Sigma-Aldrich) as the metal sources. Acetylacetonone $\text{C}_5\text{H}_8\text{O}_2$ (acac) ($\geq 99.0\%$, Sigma-Aldrich) was used as chelating ligands to reduce reactivity of the metal alkoxides. Benzene-1,4-diol $\text{C}_6\text{H}_6\text{O}_2$ (Hy) ($\geq 99.0\%$, Sigma-Aldrich) was used as the carbon source and n-butanol $\text{C}_4\text{H}_9\text{OH}$ ($>99\%$, Aldrich) was used as a solvent. For the preparation of TiC-ZrC precursor reagents molar ratio were respectively (Ti;Zr;acac;Hy) 1:1:4:1. The chemicals were used as received for except of n-butanol that was further purified by distillation over CaH_2 to remove all water. The TiC-ZrC and TiC/MWCNT polymeric precursor sol was synthesized under argon (Ar) flow in a three-neck flask to prevent a premature gelation of a metal alkoxide. As the first step of preparation of the polymeric precursor $\text{Ti}(\text{OC}_4\text{H}_9)_4$ and $\text{Zr}(\text{OC}_4\text{H}_9)_4$, were dissolved in 2 ml butanol. Then acac was dropped to the solution heated to 50°C and stirred for 30 min. The next step was increasing the temperature of the solutions up to 80°C and addition of dissolved 0.5 mol benzene-1,4-diol in 2 ml butanol. The solution turned deep red and was further heated up to a reaction temperature (125°C) and held there for 2 h. Afterwards, the solvent was evaporated at this temperature. Evaporation of solvent from polymeric precursor sol led to a neat exogels precursor, which was then pyrolysed and finally carbothermally reduced.

For the synthesis TiC/MWCNT, MWCNTs were dispersed in 1-butanol using polyvinylpyrrolidone (PVP) as a surfactant. The molar ratio of surfactant/MWCNTs was 10:1. Three solutions were made: 0.5%wt, 1wt%, 3wt% MWCNTs (weight percentage derived from carbide's final mass). All solutions were treated with an ultrasonic probe (UP 200S, amplitude 50%, cycle 0.5) for three hours. Precursor reagents molar ratio for the synthesis of TiC were respectively (Ti;Hy) 1:0.5 and followed same synthesis steps like described for TiC-ZrC precursors. In this case adding acac was not necessary because titanium (IV) n-butoxide is less reactive than zirconium (IV) n-butoxid. The MWCNT dispersion was added to the titanium (IV) n-butoxide solution before carbon source. After adding MWCNT dispersion followed by an ultrasonic treatment with an ultrasonic bath (*Elmasonic P 30H*, power 70%, frequency 37 kHz) for one hour to disperse MWCNT homogeneously in the titanium alkoxide solution. The overall synthesis process is illustrated in Figure 6.

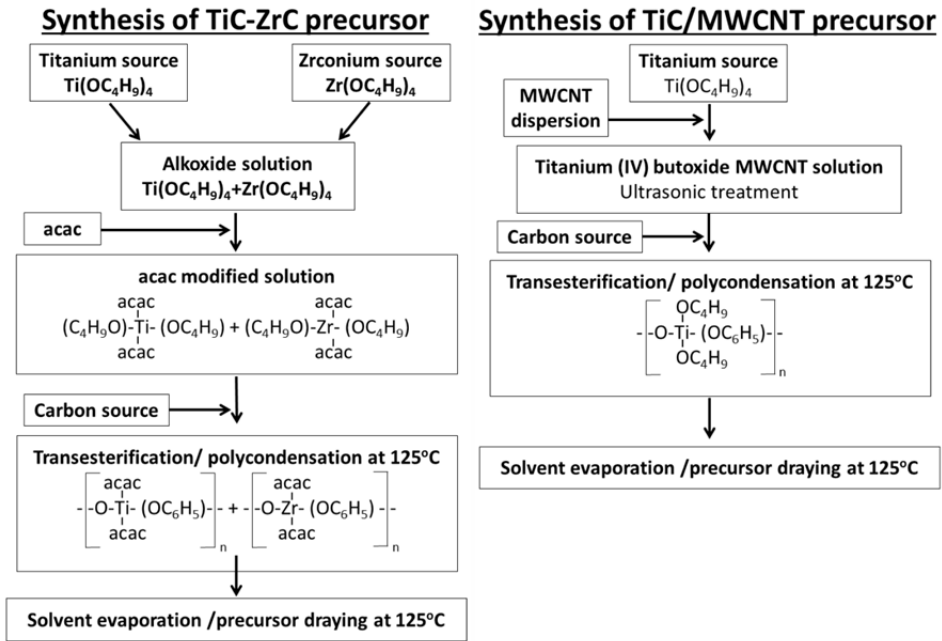


Figure 6. Flow charts of synthesis of TiC-ZrC and TiC/MWCNT precursor by sol-gel method.

The exogels were first pyrolyzed in graphite boats using an alumina tube furnace (*Nabertherm HTRH*) at $900^\circ C$ in argon for 1 h. The pyrolysed TiC-ZrC and TiC/MWCNT precursors were carbothermally reduced correspondingly at $1600^\circ C$ and $1350^\circ C$ in vacuum of $7-8 \cdot 10^{-2}$ mbar in a furnace (*WEBB 107*) for 1 h. The powder mixture of TiC-ZrC was consolidated by spark plasma sintering (SPS) using *FCT HP D25/2* equipment.

The TiC-ZrC powder was spark plasma sintered in vacuum (8 Pa) under 100 MPa uniaxial pressure at $2000^\circ C$ for 6.5 min. The heating rate was adjusted to $100^\circ C/min$ up to $1200^\circ C$ and $50^\circ C/min$ henceforth. In order to remove residual organic chemicals from the powders coming from sol-gel process degassing was carried out for 2 min at $450^\circ C$, while the pressure was kept relatively low (31 MPa) for easy removal of gases trapped within the pores. After reaching $1200^\circ C$, the pressure was increased to its maximum value (100 MPa) and kept constant until the end of the dwell period. The densification curve for the ZrC-TiC powder compacts is presented in Figure 7. More details about synthesis of ZrC-TiC and TiC/MWCNT are given in section 4.1.

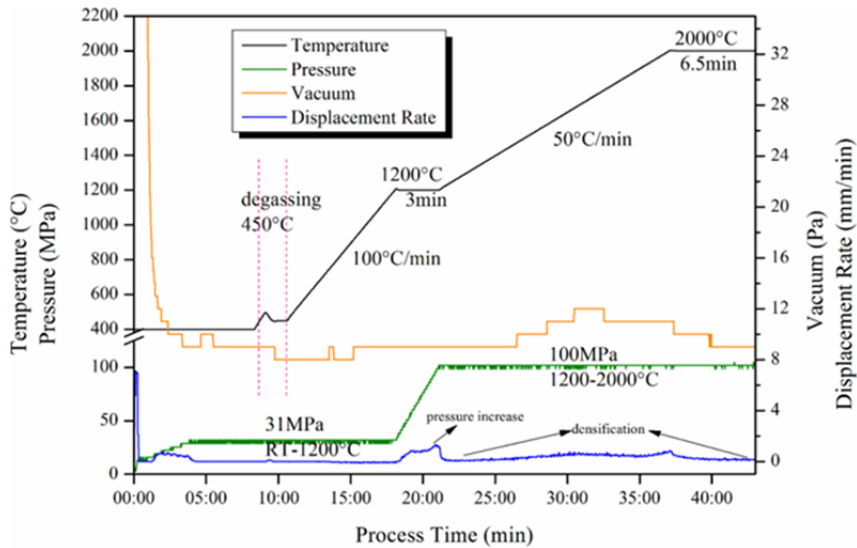


Figure 7. The densification curve for ZrC-TiC powder mixture. [V]

3.2. Synthesis of titania coatings on AgNWs network (paper IV)

TiO₂-coated AgNWs network was synthesised by spin coating technique in the framework of sol-gel method. Three different TiO₂ precursors were prepared: with HCl as catalyst, with HNO₃ as catalyst, and without any catalyst. General preparation procedure was similar for all three cases. The sol precursor was obtained by a partial hydrolysis and condensation of titanium (IV) butoxide with water, and using ethanol as a solvent. The molar ratio of water to titanium(IV) butoxide was 0.5 and the molar ratio of the catalyst to titanium(IV) butoxide was 0.05. Water and ethanol were removed by rotator evaporator (*Büchi R-114*) to decelerate the hydrolysis and condensation reaction of the sol precursor, and the concentrated sol was dissolved in hexane (10 mass%). The solution was kept overnight before deposition of titania coating onto AgNW network. AgNWs network was prepared by depositing a droplet of AgNWs-containing ethanol solution (*Blue Nano*, 1 mg/mL) onto silicon (100) substrates (10 mm x 10 mm) by spin coating at 1000 r/min for 60 s. Samples with AgNW networks were dried at 120 °C for a few minutes to remove the solvent. TiO₂ precursors were spun at 3000 r/min for 60 s onto the AgNWs network to form TiO₂ sol layer. After drying the samples were annealed from room temperatures to 600 °C in air atmosphere to burn out organic residue and turn amorphous TiO₂ layer into crystalline form.

3.3. Annealing of alumina nanofibers and AgNW sample preparation for mechanical characterisation (papers III, V)

Al₂O₃ nanofibres were purchased from *Mempro* and had diameters in the range from one hundred to few hundreds (nm) with average diameter of 156 nm and fibres length over 100 μm. An in situ SEM nanomanipulation and measurement setup was used to measure mechanical properties and monitor the response of individual Al₂O₃ nanofibres to external loading before and after annealing at 1400 °C. Al₂O₃ fibres were annealed at 1400 °C in air for 1 h, using an alumina tube furnace (*Nabertherm HTRH*). The ramping rate was 200 °C/h. Prior to the measurements the heat treated and untreated fibres were mixed in isopropyl alcohol and sonicated for 45–100 minutes in sonication bath. In order to guarantee individually dispersed nanofibers, the dispersion with very low concentration of 0.3mg/ml was prepared. Immediately after ultrasonic treatment, drop of dispersed solution containing alumina nanofibers was deposited on a TEM grid (1500 mesh copper grid, *Agar Scientific*) so that some fraction of single nanofibers were half-suspended over the mesh holes. Adhesion between the surfaces of nanofibers and copper TEM grid was sufficient to fix one end of a nanofiber to the substrate.

AgNWs solution in ethanol was purchased from *Blue Nano* and the NWs had diameters in the range from tens to a few hundreds of nanometers with the average diameter of 120 nm. A standard silicon calibration grating (TGX series, *Mikromasch*) was used as a substrate. The grating comprised of 1 mm deep square holes with 3 mm pitch. AgNWs were deposited on the grating from the solution so that some NWs were half-suspended over the holes. [89]

3.4. Sample characterization

An infrared spectrometer (Spectrum BX II FT-IR spectrophotometer, *Perkin Elmer*) was used to monitor reactions occurring during the ZrC-TiC polymeric precursor preparation. Scanning electron microscopy (*FEI Helios 600*) is used for characterization of the crystalline phases of TiC-ZrC, TiC/MWCNT composite powders, titania films and Al₂O₃ fibres, their size, structure and topography. SEM is equipped with an energy dispersive x-ray (EDX) detector (*Oxford Instruments*) and an option of focused ion beam (FIB). Mechanical characterization of individual nanofibers and nanowires nanostructures were also carried out inside SEM. Mechanical characterization experiments are described in more details in section 3.5.

The crystalline phases of all samples were examined by measuring X-ray powder diffraction (XRD) patterns and Raman spectra of samples at room temperature. The determination of the crystalline phase by X-ray diffractometer (*Rigaku SmartLab*) with Cu K α radiation at wavelength of 1.5406 Å and from

20-20° to 80° with a step width of 0.01. Quantitative Rietveld analysis was performed on the data using the AXES 2.1B program. Crystallite size τ of the samples has been evaluated by Scherrer's formula [128],

$$\tau = \frac{K\lambda}{\beta \cos\theta} \quad (12)$$

where λ is wavelength (0.15406 Å) of X-rays used, K is a dimensionless shape factor with typical value of about 0.9, but varies with the actual shape of the crystallite, β is broadening of diffraction line measured at half of its maximum intensity (in radian), and θ is Bragg's diffraction angle.

Raman spectra were recorded by spectrometer (*Reinshaw micro-Raman*) setup equipped with 514 nm continuous mode argon ion laser and the spectral resolution of approximately 1.5 cm⁻¹.

Specimen density was measured by the means of Archimedes method with distilled water as an immersing medium. The bulk Vickers hardness was estimated with *Indentec* 5030 SKV at the load of 98.1 N applied for 15 s according to ISO6507.

3.5. Mechanical characterization of individual ID nanostructures (papers: III, VI)

Cantilevered beam bending technique was used for mechanical characterization of individual Al₂O₃ and AgNWs. The method implies in-plane bending of a half-suspended object. As a result, Young's modulus and bending strength were found in both samples using two different manipulation systems inside SEM. First, Young's modulus of alumina nanofibers were measured by 3D nanomanipulator (SLC-1720-S, *SmarAct*) equipped with self-made force sensor inside SEM (Vega-II SBU, *TES-CAN*) [97]. The force sensor is made by gluing an AFM cantilever with a sharp tip (*Nanosensor ATEC-CONT* cantilevers $C = 0.2 \text{ N m}^{-1}$) to one prong of a commercially available quartz tuning fork (QTF). The sharp tip is tilted about 15° relative to the cantilever, providing visibility of the tip inside SEM [89]. During measurements, QTF was excited to its resonance frequency and the oscillation amplitude signal from it was amplified by lock-in amplifier (SR830, *Stanford Research Systems*) and recorded through an ADC-DAC card (*National Instruments*). SEM image of an individual alumina nanofiber during cantilevered beam bending and the corresponding QTF signal were simultaneously recorded. After experiments on both nanofiber samples with the same force sensor, similar bending experiment was conducted on an AFM cantilever with known spring constant. This calibration experiment allowed to extract force data from recorded QTF signal [89] [III].

Bending strength of nanostructure was determined in HRSEM (*Helios Nanolab 600, FEI*). Bending of individual nanofibers and nanowire was done

by polar coordinate nanomanipulator (MM3A-EM, *Kleindiek*) equipped with AFM probe. Each investigate object was gradually bent until breaking, while SEM images were simultaneously taken. Elastic beam theory was applied to calculate Young's modulus and bending strength from the results of the cantilevered beam bending experiments [129]. The equation for bending profile can be written in relation to Young's modulus (E) of a bent elastic beam with area moment of inertia I and loaded at its end by a point force F as follows:

$$EI \frac{d^2\theta}{dl^2} + F \cos \theta = 0 \quad (13)$$

where l is the natural axis of the beam and θ is the angle between the tangent of the bent profile and the initial profile of the beam. Moment of inertia for an object of circular cross-section (e.g. nanofiber) I is expressed as:

$$I = I_{circ} = \frac{\pi d^4}{64} \quad (14)$$

where d is the diameter of the object. Experimental data was used to numerically fit the profile curve given by Eq. 13 to nanofiber profile from the SEM image. The value of Young's modulus was extracted as described in more details in [130]. Maximum stress in a bent beam before fracture (bending strength, σ_{st}) can be found as:

$$\sigma_{st} = \frac{E\kappa d}{2} \quad (15)$$

where κ is the curvature at which the bent beam fractures [131].

Fatigue tests on single alumina nanofibers and AgNW were performed using oscillation function of the *Kleindiek* nanomanipulator, where both relative amplitude and frequency can be changed. To avoid breaking the nanofiber and nanowires special care was taken while choosing the appropriate amplitude. The tip of the manipulator was brought into contact with the Al_2O_3 fiber and the oscillation amplitude was gradually increased until the magnitude of the nanofiber deflection was slightly less than usually required for breaking a nanofiber. In case of AgNW, oscillation amplitude was increased to the value close to the maximal deformation prior the plastic yield [89].

3.5.1. Development of experimental set-up

As previously referred two different manipulation set-ups for mechanical characterisation was used, which makes measurements more complicate and time consuming. Most critical issue of smaract-based system it is not suitable to

use in HRSEM since it is not UHV compatible and contains magnetic parts, which cause distortions of the image. Therefore smaract is used only in low-resolution SEM, limiting the choice of investigated materials to those with diameters not much less than 100 nm. *Kleindiek* manipulator uses polar coordinates, which adds complicity to operation. In particular retaining the height is difficult and a small mistake could ruin the sample or a sharp probe. Moreover, due to technical restrictions, *Kleindiek* is not equipped with force sensor. Therefore, to make mechanical characterisation more accurate and less time consuming a new HRSEM manipulation setup was designed and constructed.

General recommendation for nanomanipulation set-up is ease of sample change and user friendly operation. Developing of the nanomanipulation set-up for an electron microscope is more complicated because of the specific requirements for the materials and components. No magnetic components should be used in close proximity to the electron beam to avoid distortions of the image. Both samples and probes should have sufficient electrical conductivity to exclude charging effect. Manipulator details should be vacuum compatible, and detail surface should be of high processing quality, and details design should exclude closed volumes to minimize degasing and accelerate vacuum pumping. In order to minimize a thermal drift most parts of the manipulation system should have similar thermal expansion coefficients. In our case titanium was used because the body of commercially available piezoscanners was made from titanium. [102]

During designing new set-up, it was taken into account that the set-up should provide both coarse positioning (mm range) and precise (nm range) motion of the probe relative to the substrate. The combination of coarse and precise positioning gives a wide scanning area which enables placing more or bigger samples inside SEM. The coarse and fine motion setups are separated for stability and precision. The coarse movements are realized by using x-y table with precise screws, which are jointed with a stepper motors and controlled by a computer. For the precise positioning attocube modular X, Y and Z piezo-scanners, which are easy to assemble and guarantee linear motion in Cartesian coordinates, are used. The assembly drawing of a designed nanomanipulation platform is shown in Figure. 8.

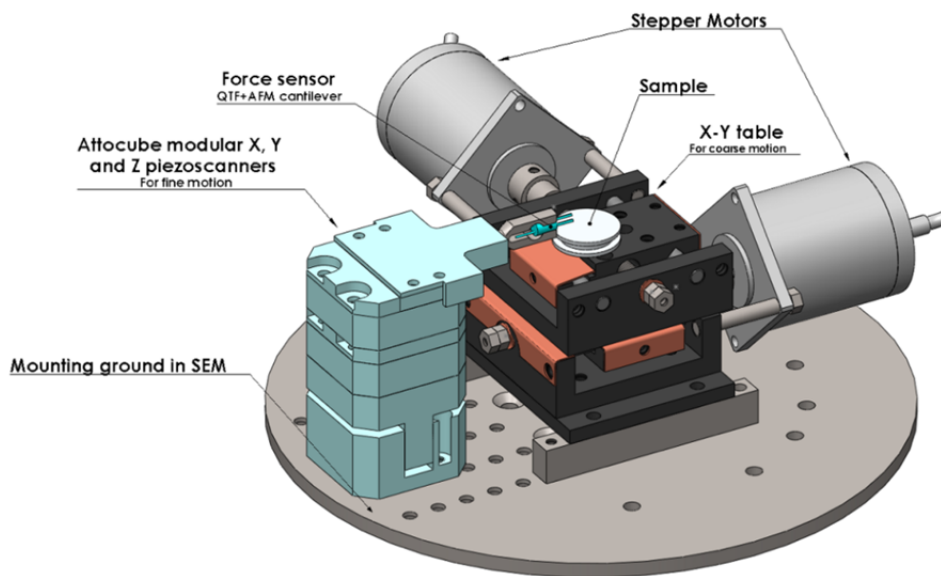
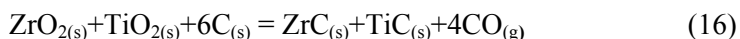


Figure 8. Constructed new nanomanipulator set-up for mechanical characterization.

4. RESULTS AND DISCUSSIONS

4.1. Synthesis of TiC – ZrC composite (papers I, II, V)

The combination of sol-gel method and carbothermal reduction was used for the first time for the synthesis of pure and homogeneous TiC-ZrC composite to improve the toughness of transition metal carbides and to reduce the synthesis temperature. In order to synthesize stoichiometric TiC-ZrC powders by the combined sol-gel and carbothermal reduction method, a molar ratio of carbon/metal oxides must be 3:1 according to the chemical equation:



Different TiC-ZrC polymeric precursors were prepared by varying the molar ratio of $\text{Ti}(\text{OC}_4\text{H}_9)_4$ - $\text{Zr}(\text{OC}_4\text{H}_9)_4$ /benzene-1,4-diol in the range of ~1:0.4 to ~1:0.95. These polymeric precursors were pyrolysed at 800 °C under argon flow. During the pyrolysis, the polymeric precursors decompose to metal oxide and amorphous carbon. Content of amorphous carbon in the pyrolysed precursor was determined by oxidative combustion in air, resulting in pure metal oxide left after burning of the amorphous carbon. The molar ratio of TiO_2 - ZrO_2 /carbon was calculated for different TiC-ZrC polymeric precursors. The results of the calculations revealed that the TiC-ZrC polymeric precursor with molar ratio of 1:0.5 metal alkoxides/benzene-1,4-diol gives the stoichiometric molar ratio for carbon/metal oxides.

An infrared spectrometer was used to monitor reactions occurring during the TiC-ZrC polymeric precursor preparation to understand metal chelate formation, transesterification and polycondensation reactions. Infrared spectroscopy was performed on the liquid precursors and dried precursors with KBr pellets. Liquid samples were pasted between the KBr windows. Solid samples were mixed with KBr powder and pressed into thin pellets.

In Figure 9. (a, b) the IR spectra of $\text{Ti}(\text{OC}_4\text{H}_9)_4$ and, $\text{Zr}(\text{OC}_4\text{H}_9)_4$ solutions in butanol shows the absorption bands at 1463 cm^{-1} and 1378 cm^{-1} due to C – H₂ and C – H₃ interactions as well as, peaks at 1154 cm^{-1} to 1020 cm^{-1} and at 600 cm^{-1} to 550 cm^{-1} assigned to Ti-O-C and Zr-O-C, interactions [132] [133]. Transesterification took place when acac was added into $\text{Ti}(\text{OC}_4\text{H}_9)_4$ and $\text{Zr}(\text{OC}_4\text{H}_9)_4$ solution, as a chelating ligand and $\text{acac}_2\text{Ti}(\text{OC}_4\text{H}_9)_2$, $\text{acac}_2\text{Zr}(\text{OC}_4\text{H}_9)_2$ were formed. IR spectra in Figure 10. at 1590 cm^{-1} and 1530 cm^{-1} due to C=O and C=C in acac groups bonded to Ti and Zr [59] [58]. The second reaction, polycondensation, occurred when carbon source benzene-1,4-diol was added to Ti and Zr alkoxide solution, where benzene-1,4-diol behaved as a bridging ligand. Benzene-1,4-diol was chosen as the bridging ligand to give an optimal stoichiometric carbon/metal ratio [59]. The solution turned deep red upon addition of benzene-1,4-diol. No remarkable changes occurred immediately in the IR spectra in Figure. 10.b after the addition of benzene-1,4-diol.

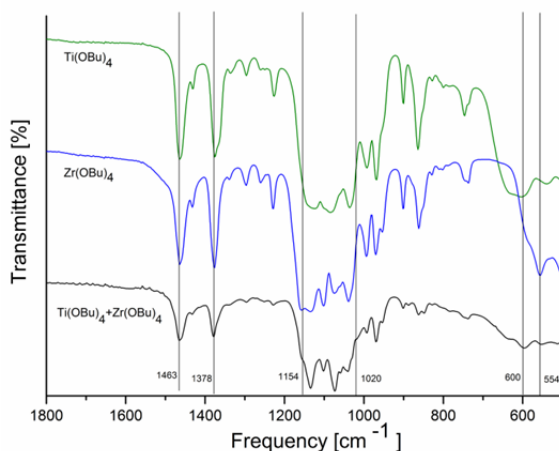


Figure 9. IR spectras of a) $\text{Ti}(\text{OC}_4\text{H}_9)_4$, b) $\text{Zr}(\text{OC}_4\text{H}_9)_4$ and c) $\text{Ti}(\text{OC}_4\text{H}_9)_4 + \text{Zr}(\text{OC}_4\text{H}_9)_4$ solution in butanol. [V]

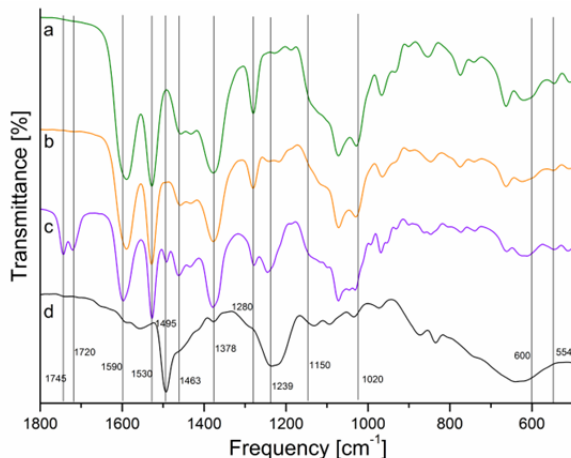


Figure 10. IR spectras of the TiC-ZrC polymeric precursor a) $\text{acac}_2\text{Ti}(\text{OC}_4\text{H}_9)_2$, and $\text{acac}_2\text{Zr}(\text{OC}_4\text{H}_9)_2$ solution in butanol; b) $\text{acac}_2\text{Ti}(\text{OC}_4\text{H}_9)_2$, and $\text{acac}_2\text{Zr}(\text{OC}_4\text{H}_9)_2$ solution in butanol after adding benzene-1,4-diol; c) $\text{acac}_2\text{Ti}(\text{OC}_4\text{H}_9)_2$, and $\text{acac}_2\text{Zr}(\text{OC}_4\text{H}_9)_2$ solution in butanol after 80 min added Hydroquinone $\text{C}_6\text{H}_6\text{O}_2$; d) dried TiC-ZrC polymeric precursor. [V]

The reaction of the polymerisation requires higher temperatures compared to transesterification, and starts at 125°C . Changes in the IR spectra occurred after an increase in the temperature up to the reaction temperature and holding at the reaction temperature for 80 min. Bands at 1745 cm^{-1} and 1720 cm^{-1} were assigned to C=O stretch that are typical for pure acac appearing in Figure 10.c [37]. Moreover, the absorption bands at 1495 cm^{-1} and 1240 cm^{-1} were assigned to benzene-1,4-diol bonded to Ti and Zr [122],[57]. Changes in IR spectra indicate that during the polymerisation some amount of the acac was substituted

by a hydroxyl group of benzene-1,4-diol. Heating of the solution up to reaction temperature resulted in solvent evaporation leading to concentrated solution and, finally, to the neat precursors. IR spectra of the neat precursor in Figure 10.d shows only the strong absorption bands at 1495 cm^{-1} and 1240 cm^{-1} which were assigned to benzene-1,4-diol bonded to Ti and Zr. Absence of the pure acac absorption bands in IR spectra indicates that it was probably removed from the precursor by evaporation. The IR measurement conformed that carbon concentration in polymeric precursor depends on the quantity of benzene-1,4-diol and the rate of polycondensation reaction.

To reduce carbide precursor to carbides powders it is necessary to carry out the energy consuming carbothermal reduction reactions at relatively high temperatures $1600\text{--}2000\text{ }^{\circ}\text{C}$ in inert atmosphere. For optimizing the carbothermal reduction parameters, i.e. to lower the reduction temperatures, I clarified the mechanism of carbothermal reduction of TiC-ZrC polymeric precursor in argon and vacuum environments at different reaction temperatures. To study carbothermal reduction process of the TiC-ZrC powders XRD analysis was carried out on the samples reduced at temperatures of $800\text{ }^{\circ}\text{C}$, $1100\text{ }^{\circ}\text{C}$, $1300\text{ }^{\circ}\text{C}$ and $1500\text{ }^{\circ}\text{C}$ in argon and vacuum. Figure 11. shows XRD patterns of samples annealed in argon and vacuum at different temperatures.

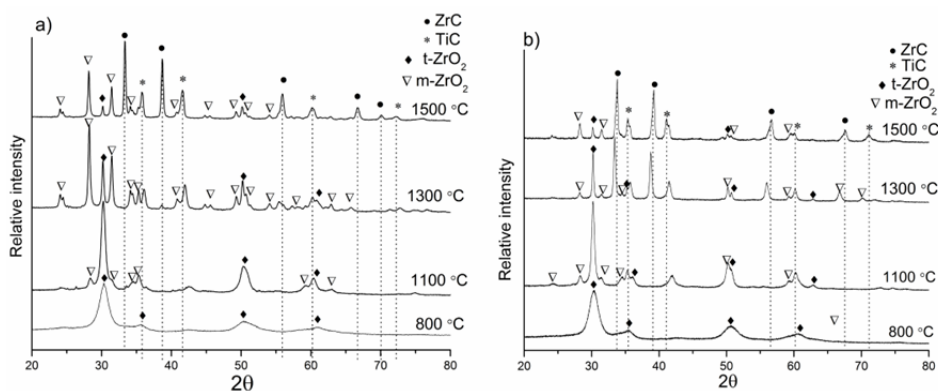


Figure 11. X-ray diffraction patterns of a) ZrC-TiC polymeric precursor reduced in argon; b) ZrC-TiC polymeric precursor reduced in vacuum. [II]

XRD results for the heat treated sample at $800\text{ }^{\circ}\text{C}$ in argon and vacuum are similar and show strong and broad diffraction peaks at 2θ : 30.24° , 35.48° , 50.65° , 60.22° pointing the fine tetragonal zirconia ($t\text{-ZrO}_2$) crystallites (ICDD No.: 01-079-1764). The XRD analysis detected no peaks corresponding to titania phases. This may be due to extremely fine TiO_2 crystallites that can be hardly detected by XRD or very low volume fraction of TiO_2 that cannot produce XRD peaks that are discernible above the background signal. The broad diffraction peaks can also indicate the presence of titanium and zirconium binary oxides ($\text{Ti}_{0.5}\text{Zr}_{0.5}\text{O}_2$) according to (OCD No. 96-100-8791). These board

diffraction peaks make it difficult to accurately identify a phase since Raman spectroscopy was used to clarify this sample composition. Fig. 12 shows Raman spectrum of the sample of the ZrC-TiC polymeric precursor pyrolysed at 800 °C in vacuum. In the spectrum two strong peaks at approximately 1340 cm^{-1} and 1590 cm^{-1} are clearly recognized. These peaks can be associated with the A_{1g} and E_{2g} vibrational modes of carbon [134]. The spectrum shows also five broad peaks at approximately 153, 288, 340, 421, 640, and 767 cm^{-1} . These peaks are comparable to the reported Raman spectra of titanium and zirconium binary oxides (TiO_2 - ZrO_2) in the literature [135], [136]. Therefore, one can conclude that sample of the ZrC-TiC precursor pyrolysed at 800 °C consists of TiO_2 - ZrO_2 mixed oxides and amorphous carbon. XRD patterns do not show any carbon peaks because amorphous carbon have no diffraction peaks.

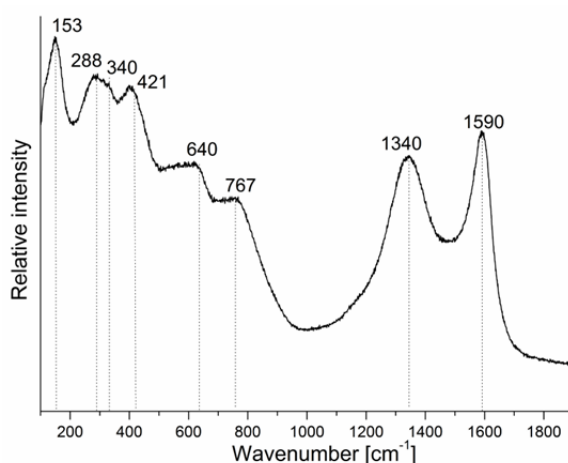


Figure 12. Raman spectrum of ZrC-TiC precursor heated at 800 °C in vacuum [I]

The XRD patterns show differences for the samples heat treated at above 800 °C in argon and in vacuum environments Figure 11. The mean difference at 1100 °C is that in the vacuum heat treated sample the pattern shows weak TiC diffraction peaks (ICDD No.: 00-900-8747). Meanwhile in argon heat treated samples intensity of t- ZrO_2 peaks is increased that may indicate transformation of some amount of t- ZrO_2 to monoclinic zirconia (m- ZrO_2) (ICDD No.: 01-081-1314). However, TiC peaks appear in the heat treated samples in argon at 1300 °C. The formation of ZrC particles is noticed in the sample treated at 1300 °C in vacuum and in the samples treated at 1500 °C in argon according to (ICDD No.: 01-077-7214). Heat treatment at 1500 °C in both cases resulted in development of ZrC and TiC predominant phases but still containing small amount of ZrO_2 phases. However, XRD pattern for the heat treated sample at 1500 °C in vacuum shows that intensity of ZrO_2 phases is lower than that for the sample treated in argon. The XRD analysis has shown that the carbothermal reduction of the binary solid carbide mixture (ZrC-TiC) polymeric precursor

started in vacuum at lower temperature (1100 °C) than in argon environment. The temperature of reaction between metal oxide and amorphous carbon particles (Eq. 19) decreases when the system pressure decreases [37]. Therefore, the preparation of metal carbide in vacuum is easier than that at atmospheric pressure. In vacuum the CO gas is ejected faster during carbothermal reduction and carbides forms more easily than in argon. Therefore, in order to reduce the residue of ZrO₂ to ZrC a subsequent carbothermal reduction at 1600 °C in vacuum was carried out. By 1600 °C, two major phases are detected by XRD cubic zirconium carbide with a lattice parameter of 4.657 Å and titanium carbide with a lattice parameter of 4.342 Å. However, the XRD pattern (Figure 13) of the samples carbothermally reduced at 1600 °C in vacuum still detects the very weak peaks of monoclinic ZrO₂ and indicates the blended compounds consisting of pure TiC, ZrC phase and 2.2 wt% of monoclinic ZrO₂ phase. The grain size analysis gives the powder mean grain size of 133 nm +/- 32 nm. It indicates a high level of particles agglomeration with the agglomerate sizes ranged between 1 and 5 µm. The crystallite size of the samples reduced at 1600 °C has been evaluated by Scherrer's relation and found to be 50 nm for TiC, 26 nm for ZrC and 63 nm for m-ZrO₂, respectively.

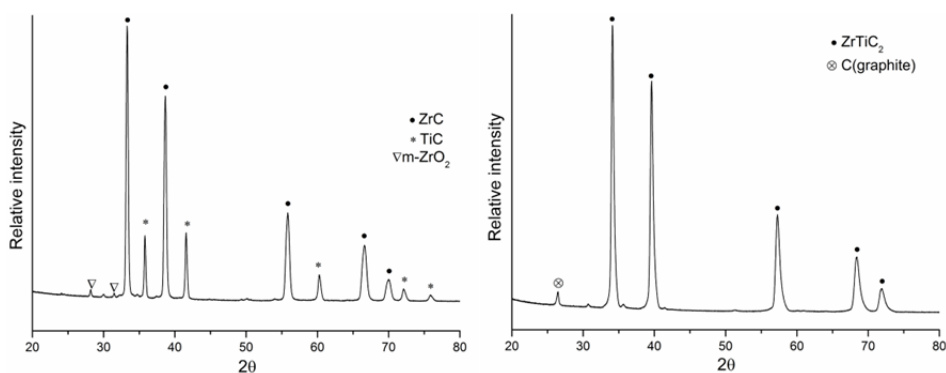


Figure 13. a) XRD pattern of the precursor powders carbothermally reduced at 1600 °C and b) XRD pattern of the sintered ZrTiC₂ solid solution. [V]

For densification the synthesised TiC-ZrC powder to a bulk solid specimen, the powder is first pressed (20 MPa) to the required shape and secondly sintered at 1700 °C for 25 min. The density measurements by Archimedes technique resulted in 4.2 g/cm³ which indicate its high porosity. SEM images of the porous specimen are shown in Figure 14. The previous attempts to sinter the samples at higher temperatures with the above-described sintering setup have failed. Taking into account the fact that TiC-ZrC system forms a miscibility gap at around 2000 °C, the SPS method was used and sintering temperature was adjusted to 2000 °C for development of the stable single-phase solid solution of TiZrC₂. Because the temperature of sintering was high enough for decomposition of carbides, the process of consolidation took place in the single-

phase region. The XRD pattern shows a single-phase material, cubic ZrTiC_2 (ICDD No. 01-077-7207) (Fig. 12), with the lattice parameter of 4.547 Å. However, it should be mentioned that insignificant amount of free carbon in graphite polymorph was also detected.

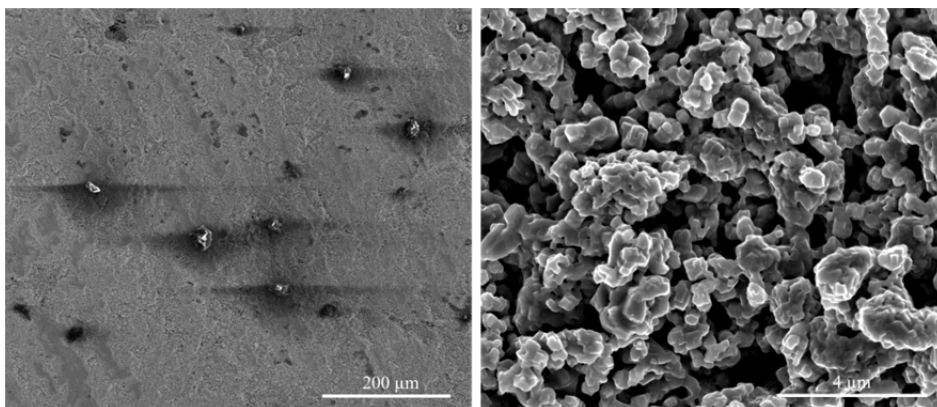


Figure 14. SEM Images of porous TiC-ZrC specimen sintered at 1700 °C.

Hardness and indentation fracture toughness were found to be $\text{HV5} = 2244 \pm 64$ and $3.2 \pm 0.7 \text{ MPa m}^{1/2}$, respectively. The calculated Young modulus was $342 \pm 33 \text{ GPa}$. As the calculation of fracture toughness was based on determination of crack patterns, i.e. according to Palmqvist crack mode, the specimen was thoroughly polished with 1 μm diamond paste. The bulk density of the material, measured by Archimedes technique, was 5.965 g/cm^3 . Because of uncertainties in the composition, the theoretical density was not calculated for the solid solution. However, image analysis suggests around 2 % of residual porosity that may be slightly overestimated due to chipping around existing pores or voids during polishing. The micrograph displayed in Fig. 15. shows the fracture mode operating in the material. At room temperature, the fracture of transition metal carbides and their alloys is usually considered as brittle intergranular fracture with crack propagation mechanism described by Griffith's theory of fracture. However, the ZrTiC_2 solid solution exhibits a mixed fracture mode with inter- and intra-granular cracking together with plastic grooving. The fracture surface contains a large number of structural elements, which indicate the plasticity in micro-volumes of the material.

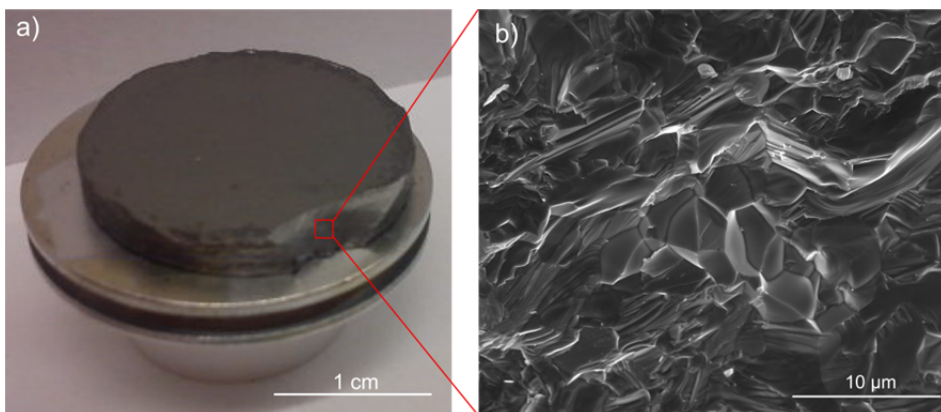


Figure 15. Photo of TiZrC_2 specimen by SPS b) SEM image of ZrTiC_2 fracture surface. [V]

In our case the sample is made by sintering at $2000\text{ }^\circ\text{C}$ resulting in TiZrC_2 single-phase material and exhibits mechanical properties comparable with other similar materials as shown in Table 2 on page 6. This comparison shows that by combined sol-gel and carbothermal reduction method it is possible to synthesize TiC-ZrC powders for fabrications single-phase carbides.

4.2. Synthesis of TiC/MWCNT composites powders

In order to elaborate MWCNT reinforced CMC to improve transition metal carbide toughness it is necessary to solve three critical issues: 1) homogeneous dispersion of CNTs in the matrix, 2) optimization of the interfacial bonding between CNTs and adjacent matrix and 3) development of novel consolidation methods that do not damage the CNTs. It is crucial that the carbon nanotubes are homogeneously dispersed in the matrix system, while presence of agglomerates can act as a point defect and lead to dispersion failure [66]. In this section synthesis of TiC/MWCNT composites by combined sol-gel and carbothermal reduction method is described. The most critical issues of this topic are MWCNT resistance to carbothermal reduction and achieving homogeneous dispersion of MWCNT. TiC was chosen as matrix material because the synthesis temperatures are lower than for ZrC as shown in the previous section.

Samples with three different concentrations of MWCNT wt% (0.5%, 1%, 3%) were prepared to clarify morphology and distribution of the MWCNTs in TiC matrix. PVP was used as surfactant following Q.Y. Tang et al. [72]. They have shown that PVP gives a stable CNT dispersion for at least two months. PVP forms a reversed micelle around a CNT, the molecular chain of the PVP is adsorbed and wrapped on the CNTs randomly and ultrasonic treatment provides strong shearing forces between CNTs. CNTs covered with such polymers could react with polycondensate titanium (IV) butoxide by benzene-1,4-diol, and CNT

surface has been coated with TiC precursor. One possible way to form such coating is through hydrogen bonding interaction between a carbonyl group of PVP chains and the hydroxyl group. This results from the polycondensation reaction of titanium (IV) butoxide [137], [138]. Thus the PVP behaves as polymer glue between MWCNT and TiC carbide precursors, as illustrated in Figure 16.

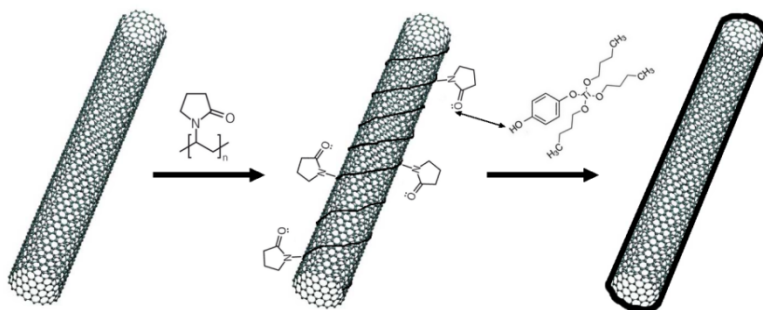


Figure 16. Schematic illustration of the process of preparation of TiC/MWCNT precursor.

The MWCNT/TiC composites were prepared by carbothermal reduction at 1350 °C from polymeric precursor. X-ray spectroscopy was used to characterize the composition of MWCNT/TiC composites. Figure 17. shows XRD pattern of TiC with different concentrations of MWCNT, where they all exhibit characteristic diffraction peaks of TiC (ICDD No.: 00-900-8747) at $2\theta = 35^\circ$, 41° , 60° , 72° and 76° . XRD spectrum of the sample with 1% nanotubes is the only that shows weak and board diffraction peaks of rutile and anatase phase of TiO_2 at 2θ : 25° , 27° and 54° . The TiO_2 presence is due to combustion of the sample in air after carbothermal reduction, which resulted in oxidation of small TiC particles to TiO_2 .

Raman spectroscopy was used to find out whether the sample contains multiwalled carbon nanotubes. The results were compared with the literature data [139], [140] and the spectrum of commercial TiC (*Pacific Particulate Materials Ltd*, 99,7%). Raman spectroscopy enabled to distinguish between carbon nanotubes and other carbon allotropes. In the Raman spectrum of carbon there are three characteristic peaks at about 1350 cm^{-1} , 1590 cm^{-1} and 2700 cm^{-1} . The width, intensity and Raman shift of these peaks depended on the structure of carbon. The peak at 1350 cm^{-1} , called D peak, indicates the defectiveness and structure of graphitic materials. G- peak, at about 1590 cm^{-1} , is assigned to in-plane vibration of the C–C bond [141]. The band at 2700 cm^{-1} is an overtone of the D band and called G' band. G' band is an intrinsic property of the nanotube and graphite, and present even in defect-free nanotubes for which the D band is completely absent.[142] The I_D/I_G ratio shows a disorder in nanotube structure and is a good indicator of the quality of nanotubes.

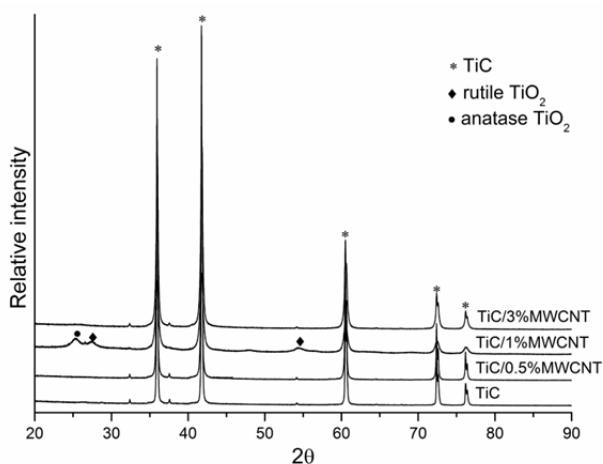


Figure 17. XRD pattern of TiC/MWCNT composite powders synthesized by carbothermal reduction.

Raman spectra of the samples were measured in the range of $100\text{--}3200\text{ cm}^{-1}$ from multiple locations on each sample to evaluate its homogeneity. The laser excitation intensity of Raman spectrometer was decreased to avoid damaging of MWCNTs. The peaks of different samples are not notably shifted, but their intensities and widths vary. The variations in peak widths and intensities of samples can be caused by the irregular position of the particles on the glass substrate [139]. It may also indicate that powders are not so homogeneous and pure. In Figure 18. at 150 cm^{-1} , 260 cm^{-1} , 420 cm^{-1} and 605 cm^{-1} there are broad peaks, which are due to the disorder induced by carbon vacancies [143]. Stoichiometric TiC cannot be characterized by Raman spectroscopy because it is not Raman active [139]. The characteristic bands of nanoscale carbon (G and D) can be seen in both Raman spectra, the commercial sample and the synthesized one in Figure 18. (a, b), which indicate that the samples contain excess carbon. The XRD analysis does not show a noticeable amount of carbon, because there is no peak characteristic to carbon. In the Raman spectra of TiC/MWCNT samples in Figure 18.d,e,f the D and G peak intensities are increased and G'-band appears in the spectra, which indicates the existence of MWCNT in the samples. By comparing the Raman spectra of pure CNTs in Figure 18.c and TiC/MWCNT samples in Figure 18d,e,f, it can be seen that D band intensity has increased which indicates that the number of defects in MWCNTs has increased during the sample preparation. At first sight it can be concluded that during the synthesis of TiC/MWCNT composites MWCNTs are damaged. It should be taken into account that samples in Figure 18.d,e,f may contain excess nano-carbon like the sample of pure TiC in Figure 18b. The Raman active bands of carbon and MWCNTs are combined in the spectrum and thus do not describe the quality of nanotubes. The variety of intensities and widths of Raman active bands also complicate the characterization.

Unfortunately no reliable information about the samples can be acquired from the spectra.

SEM was employed for structural characterization of TiC/MWCNT composite powders. SEM images of TiC with three different concentrations of MWCNT wt% (0,5% 1%, 3%) composite powders are shown in Figure 19. As one can see, SEM characterization confirms that MWCNTs are present in TiC powders after carbothermal reduction in all samples. At low concentration of MWCNTs they are well-distributed in matrix and there are only few nanotube aggregates Figure 19.b,c.

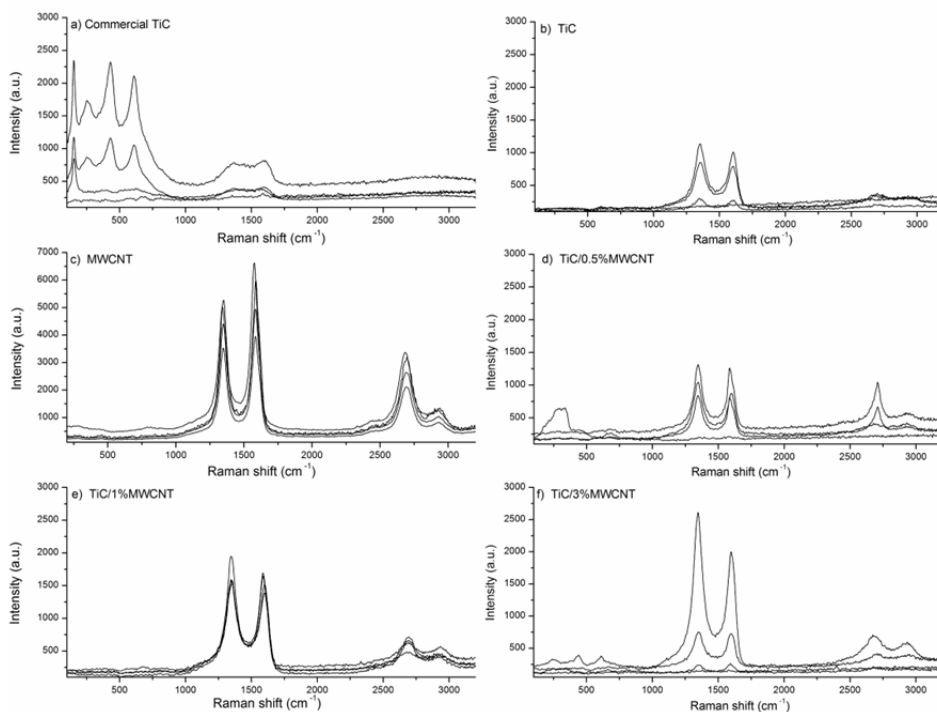


Figure 18. Raman spectra of: (a) commercial TiC; (b) TiC; (c) MWCNT; (d) TiC / 0.5% MWCNT composite; (e) TiC / 1% MWCNT composite; (f) TiC / 3% MWCNT composite.

Due to lightness of CNTs mass 3% of carbon nanotubes in the matrix is relatively high and nanotubes are agglomerated Figure 19.d. In Figure 19.a the overview of typical structural and morphological composition of TiC and TiC/MWCNT powders is presented. The grain size of the powders typically varied from 300 nm to 500 nm and some grains are agglomerated to form bigger particles with size ranging from 1 μm to 3 μm .

EDX measurements were carried out to evaluate concentration of the excess carbon in synthesized samples. The EDX measurements of the same samples confirmed the results of Raman's characterization and showed that all samples

contained a small amount of excess carbon. The calculation based on the EDX results demonstrates that pure TiC sample contained 1% wt, TiC/0,5%MWCNT contained 1,8% wt and TiC/3% MWCNT contained 2,8 % wt of excess carbon. The TiC/1%MWCNT sample did not contain excess carbon but did contain a small amount of oxygen because of the combustion. The characterization of the samples shows that the combination of sol-gel method and carbothermal reduction is a promising method to synthesize carbon nanotubes reinforced carbide composites. The synthesis process of TiC and TiC/MWCNT composite has to be optimized to avoid formation of excess carbon.

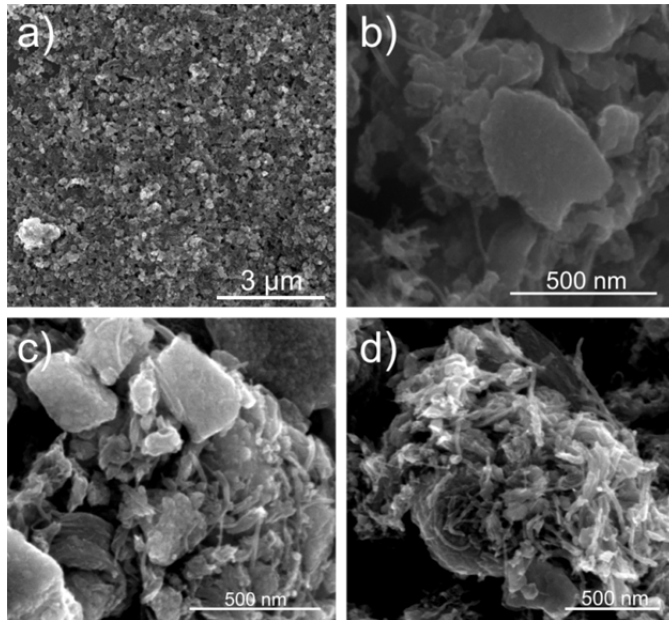


Figure 19. SEM images of a) typical TiC and TiC/MWCNT powders b) TiC/0.5%MWCNT, c) TiC/1%MWCNT, d) TiC/3%MWCNT.

4.3. Mechanical characterization of annealed Al_2O_3 nanofibers (paper VI)

Metal oxides nanofibers would be a very attractive reinforcement material in all sorts of composite materials, but especially in UHTCs matrix composites where polymer fibers, carbon fibers and MWCNT could be damaged due to high processing temperatures. Alumina nanofibers are a potential composite reinforcement agent due to high strength and elastic modulus, low thermal conductivity and chemical stability [144]. The nanofibers should withstand the high temperature in processing of CMCs without significant alteration in morphology/structure or mechanical properties. Coupled thermal analysis on commercially available alumina nanofibers showed substantial change in surface morphology

and phase at 20–1480 °C [145]. Alumina fibers have taken in form of more agglomerated/partially sintered cell shape with small pores (~50–200 nm) between them. This kind of structure change may give drawbacks during preparation of CMCs. In order to prevent faults during preparation of CMCs that are caused by decomposition of reinforcement agent it is crucial to reveal changes of structural and mechanical properties of alumina nanofibers before and after heat treatment. This section describes applicability of commercially available (*MemPro Ceramics*) alumina nanofibers as a reinforcement material in CMCs like metal carbides or oxides composites. *In situ* cantilevered beam bending technique is used for mechanical testing (described in section 3.5.) of untreated and annealed nanofibers at 1400 °C.

SEM was employed for structural characterization of untreated and annealed alumina nanofibers. SEM images of untreated and annealed alumina nanofibers before and after dispersing are shown on Figure 20. No change in nanofiber diameter was observed after the annealing. After dispersing the fibre mat decomposed to individual nanofiber with length up to 5 µm. Average length of individual annealed nanofibers was smaller which could be explained by apparent fusion of intersecting nanofibers. As can be seen in Figure 20d, many of the intersecting nanofibers stayed together after dispersion forming a branch-like structure. Although melting point of *Mempro* alumina nanofibers is above 2032 °C it has been shown that intersecting nanofibers soften and form interfiber bonds at lower temperatures [146]. This effect could be advantageous for preparation of CMCs and may lead the better interfacial bonding between fibres and matrix material. These interfacial bondings prevent sliding out fibres from matrix under load and results in higher toughness of material.

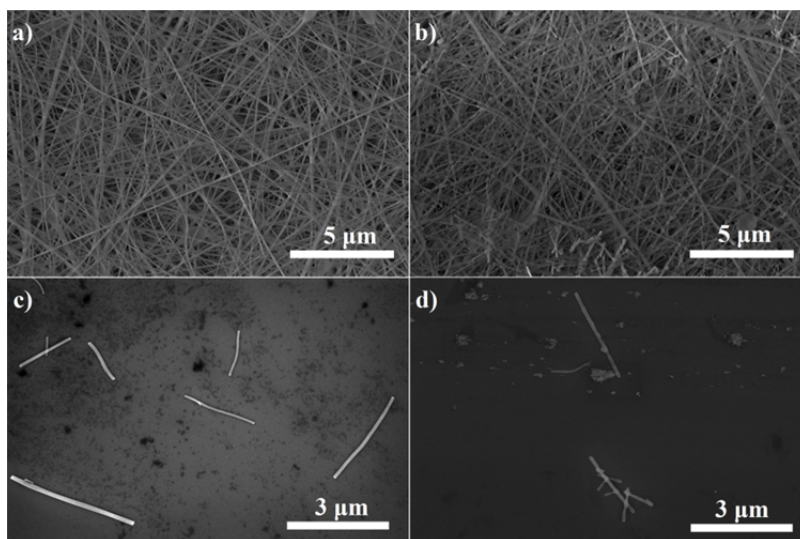


Figure 20. SEM images of untreated (a,c) and annealed (b,d) alumina nanofibers before and after dispersing. [VI]

Crystal phase of untreated and annealed alumina nanofibers were determined using XRD. XRD patterns for both samples are presented on Figure 21. All the broad diffraction peaks on the XRD pattern (b) of untreated nanofibers can be identified as cubic γ - Al_2O_3 (OCD No. 2015530). The XRD pattern of annealed nanofibers (a) shows strong and sharp peaks due to hexagonal α - Al_2O_3 phase (OCD No. 1000032). The XRD analysis indicates that the phase transition of γ -alumina to α -alumina takes place below 1400 °C which is consistent with the previously reported results [147],[148].

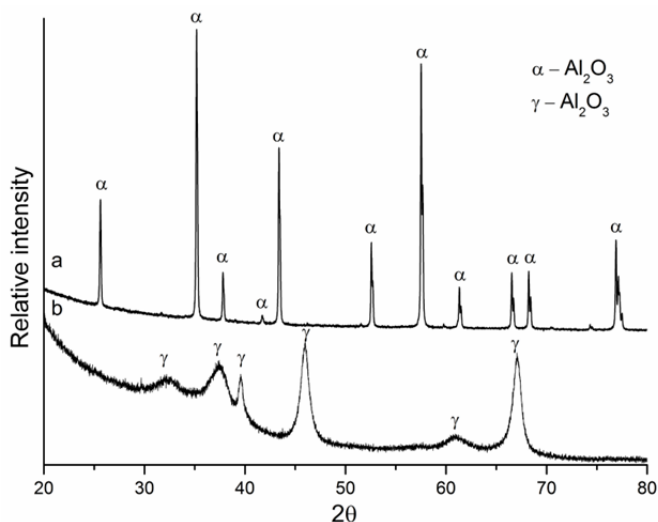


Figure 21. XRD patterns of the α -alumina (a) and the γ -alumina (b) nanofibers with their characteristic peaks. [VI]

The beam bending tests were performed to evaluate mechanical properties of Al_2O_3 nanofibers. Measurement of Young's modulus was conducted on 18 untreated and 12 annealed alumina nanofibers with radii between 57.9 nm and 129.0 nm. Median Young's modulus value for untreated nanofibers was found to be 143 ± 38 GPa. Experiments on annealed nanofibers showed almost twice as high Young's modulus values with the median value being 245 ± 35 GPa. Both these values are lower compared to reported Young's modulus for bulk alumina (370 GPa) [149]. Lower values for oxide nanofibers produced by electrospinning can be explained by effect of crystal orientation, diffusional creep at room temperature and neglected shear deformation [150]. Higher Young's modulus values for annealed nanofibers compared to untreated nanofibers may be caused by higher crystallinity of α -phase that lead to improvement in mechanical properties [151]. The increase of crystallinity can be seen from the XRD patterns on Figure 21, where the α -phase has sharp peaks as opposed to wide and low intensity peaks of the γ -phase.

Similarly to Young's modulus measurements, bending strength test was carried out on untreated and annealed alumina nanofibers. In both cases 18

nanofibers with radius between 37.8 nm to 89.8 nm were bent until they broke. Median bending strength value for annealed nanofibers was two times higher than for untreated nanofibers being 11.3 ± 2.3 GPa and 5.3 ± 1 GPa. Untreated and annealed nanofibers deformed elastically until suddenly broken Figure 22. Elastic deformation was especially evident in restoration of initial shape after the AFM tip slipped while bending the nanofiber to a considerable deformation. This is a common behaviour for oxide materials, which are known to be brittle materials. Fatigue test have shown that alumina nanofibers can be bent over 1 million cycles without visible signs of deformation or fracture.

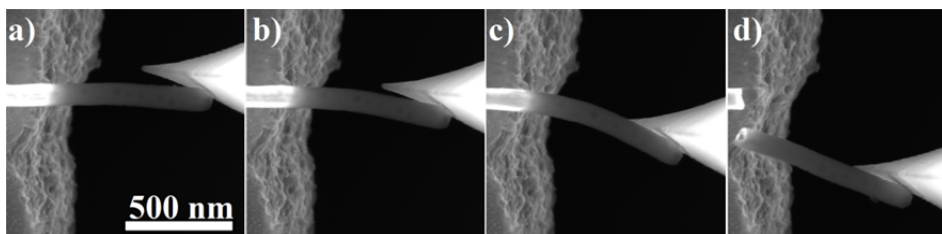


Figure 22. Bending strength test on annealed alumina nanofiber. AFM tip is first brought into contact with nanofiber (a) and then gradually bent (b–c) until it breaks (d). [VI]

Based on mechanical and structural characterization one can conclude that commercially available (*MemPro Ceramics*) alumina nanofibers are suitable for fabrication of CMCs temperature up to 1400 °C. In order to assess *MemPro Ceramics* alumina nanofibers as reinforcement in ceramic matrix further experiments with specific matrix material and conditions are required.

4.4. Preparation of titania and Ag NW random network functional coatings by sol – gel method (papers III, IV)

As described in section 1.3. AgNW is a promising material for flexible transparent electrodes and nanoelectromechanical systems (NEMS) due to their excellent electrical and thermal conductivity, perfect structure, and ease of synthesis. Besides the electrical and optical properties, mechanical characteristics are also of a great importance for performance of the named systems. In particular, NWs should withstand numerous repetitive deformations. Therefore elasticity, plasticity, fatigue and fracture of AgNWs need to be characterised. However, such NEMS and electrodes may fail due to corrosion of AgNWs exposed to ambient conditions, which adversely affects the conductivity of AgNW network [152]. Another reason of failure of such systems is instability of AgNWs at elevated temperatures caused, e.g. by electrical current [88]. Coating of AgNWs network with thin oxide layer could protect them from the corrosion and enhance the thermal stability [90] [6]. To develop reliable flexible

transparent electrodes and NEMS) based on AgNW it is important to understand interactions between AgNW and protective coatings. This section describes mechanical properties of AgNWs by *in situ* cantilevered beam-bending technique. It is also shown that interaction between AgNW and protective oxide layer may cause undesirable effects. In addition, I have demonstrated the electron beam-induced growth of silver nanowhiskers observed in real-time in SEM on the surface of a TiO₂ layer that covers AgNWs network. The growth conditions are systematically revealed and possible growth mechanisms are discussed.

Mechanical measurements of AgNW are performed inside SEM which enables real-time visualization of NW behaviour during the measurements and fine control over the experiment. The experimental details are described in section 3.5. The beam bending tests were performed on NWs with diameters ranging from 76 nm to 211 nm. The measurements show that AgNWs have two typical deformation regions elastic and plastic. It was also confirmed separately on several NWs that within the elastic region the NW restores the undeformed state upon removal of the external force. Even the strongly bent NW has no signs of fracture, and the deformation seems to be purely plastic, indicating significant difference of AgNW behaviour in pure bending conditions in comparison to “super elastic behaviour followed by unexpected brittle failure” [98] and limited plasticity [153] reported in three point bending and tensile tests respectively. Nevertheless about one third of the NWs broke during the bending test. The broken end still remained partly attached to the rest of the NW in all of the cases of fracture, which is not typical for purely brittle fracture. Moreover, very small, but nonzero force is still detectable after fracture, which may indicate the presence of a small neck connecting two parts of the NW [89]. For calculation of mechanical properties the experimental data of the force curves and NW profiles from the SEM images were fitted to the equilibrium profile of elastic beam calculated [130].

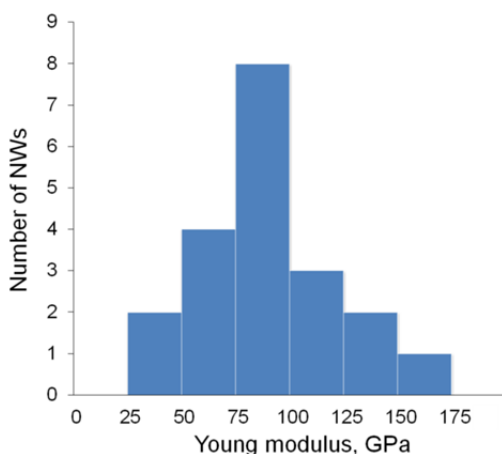


Figure 23. Distribution of Young modulus for set of 20 nanofibers [III]

Young moduli of NWs ranged from 39 GPa to 150 GPa with the median of 90 GPa, which is only slightly higher than the bulk value 83 GPa [154] of silver and is close to Young's moduli obtained by other methods for similar diameters. The median average yield strength value of NWs was of 4.8 GPa [89]. Literature data on the yield strength of AgNWs measured in pure bending tests is absent. In tensile test for the similar diameters Zhu et al. obtained a yield strength of approximately 1 GPa, which is two orders of magnitude higher than the bulk value (55 MPa) [154] and approaches the theoretical strength (3.5 GPa) of Ag in the $\langle 110 \rangle$ direction [155]. Based on mechanical tests it can be concluded that AgNWs can be bent elastically multiple times without fracture and therefore are suitable for NEMS applications. [III]

To develop protective layer on AgNW random network, the AgNW random network were deposited on silica substrate and covered with titania precursor by spin coating technique. To study the thermal stability of AgNW random network was coated partial hydrolysed and condensed titania precursor. Samples were annealed in a furnace (Nabertherm HTR70-150/13) for 30 min at 5 different temperatures: 200 °C, 300 °C, 400 °C, 500 °C, and 600 °C. Ramping rate was 1.7 C/min. Typical SEM images of the samples annealed at different temperatures are given in Figure 24. For the sample annealed at 200 °C for 30 min, cracks formed in TiO₂ layer at the places above AgNWs (Figure 24a). Moreover, AgNWs were partly decomposed leaving wire-shaped patterns inside TiO₂ layer. At 300 °C the decomposition of AgNW was more pronounced and silver atoms diffused into the TiO₂ layer resulting in fine particles of silver formed onto the surface and inside the TiO₂ layer (Fig. 24b). At 400 °C most of AgNWs were decomposed (Figure 24.c). The annealing at 500 °C and 600 °C resulted in complete decomposition of all AgNWs (Figure 24.d).

In the process of SEM characterization of the sample annealed at 400 °C an intensive spontaneous growth of Ag whiskers from the TiO₂ layer was observed. The growth was activated by electron beam focused on the area of interest. The growth was observed mostly from the areas where AgNWs were clearly visible below the TiO₂ film (Figure 25.). Some whiskers grew also in vicinity of AgNWs and at the areas where AgNWs were decomposed. Diameters of whiskers varied from a few (nm) to several hundred (nm). Most of the whiskers had circular cross-section, while some whiskers possessed irregular geometry (Figure 25.b). At the electron beam parameters of 10 kV voltage and 0.34 nA current the growth rate was up to several tens of (nm/s). An average growth time until the growth termination was approximately 30 s. Variation of the electron beam parameters (voltage from 5 kV to 30 kV and current from 5.4 pA to 5.5 nA) had no noticeable effect on the growth.

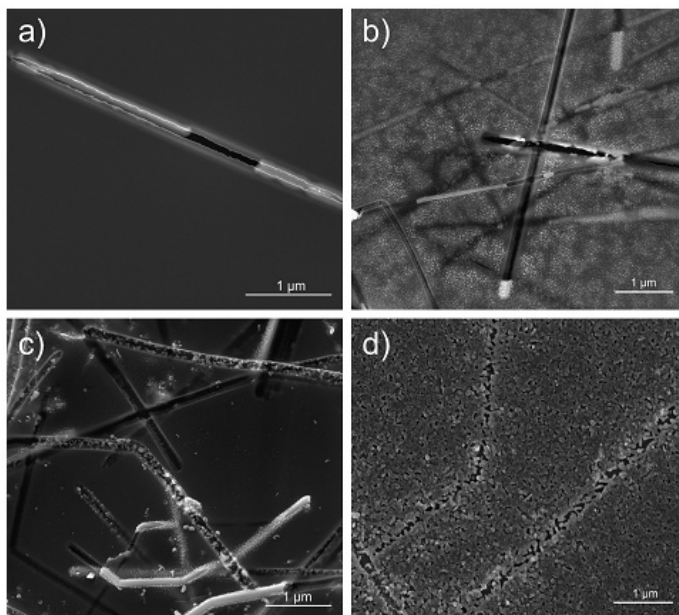


Figure 24. SEM image of AgNW network on silicon substrate covered with TiO₂ layer annealed at (a) 200 °C, (b) 300 °C, (c) 400 °C and (d) 600 °C. [IV]

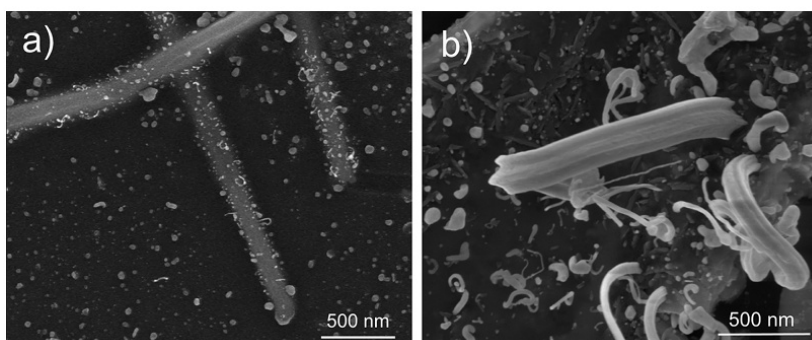


Figure 25. SEM images of electron beam induced growth of Ag whiskers from the TiO₂ coated AgNWs network annealed at 400 °C for 30 min, typical whiskers (a) and irregular whiskers (b). [IV]

In order to investigate the mechanism of Ag whiskers growth more precisely, the second annealing series at 400 °C for 5, 10, 30, 60 and 180 min were carried out. For the sample annealed for 5 min some AgNWs were partly decomposed and Ag diffused into the TiO₂ layer Figure 26.a. No whiskers growth was observed. For the sample annealed for 10 min the growth of a few single whiskers was observed Figure 26.b. On the samples annealed for 30 Figure 26.c and 60 min the whisker growth was intensive. After annealing for 180 min all AgNWs were decomposed and no whiskers were observed Figure 26.d.

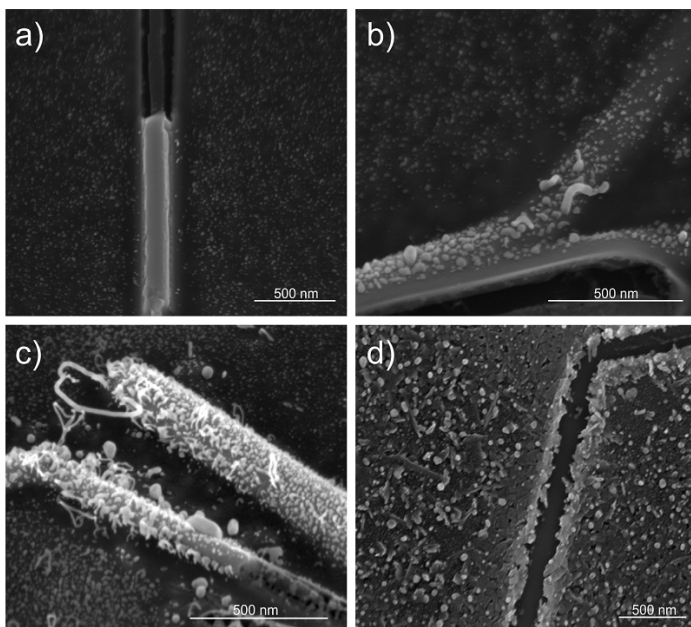


Figure 26. SEM image of AgNW network on silicon substrate covered with TiO₂ layer annealed at 400 °C for various times (a) 5 min, (b) 10 min (c) 30 min and (d) 180 min. [IV]

In addition, dependence of the whiskers growth on TiO₂ layer thickness was investigated. It was found that the whiskers appear when the coating thickness ranges from 50 to 200 nm. For thinner and thicker coatings no growth was observed. Aging experiments were carried out as following. Two samples were kept at ambient conditions for half year and were characterized in SEM once per week. Every time the whiskers growth was observed.

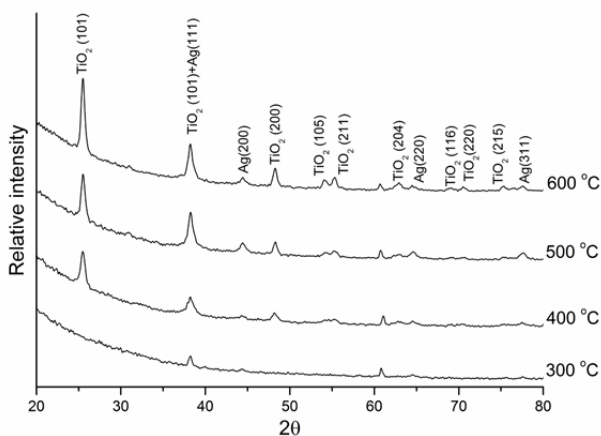


Figure 27. GIXRD patterns of the Ag NWs network on silicon substrate covered with TiO₂ layer and annealed at different temperatures. [IV]

For structural characterization of samples X-ray spectroscopy was used. The GIXRD patterns of the samples annealed at different temperatures are presented in Figure 27. Below 400 °C only silver reflexes are seen at 2θ values of 38.3°, 44.1°, 64.4° and 77.5° [128], [156] No TiO₂ reflexes are seen indicating absence of crystalline phase. Starting from 400 °C reflexes at 25.4°, 38.4°, 48.2°, 53.9°, 55.2°, 62.8°, 68.9°, 70.5°, and 77.5° start to appear that are corresponding to TiO₂ anatase phase [83] and indicating the crystallisation of TiO₂. According to Debye–Scherrer’s formula an average TiO₂ crystallite size increased from 15 nm for 400 °C to 20 nm for 600 °C. Silver reflexes are still present even after annealing the sample at 600 °C for 30 min, indicating that silver particles are distributed in TiO₂ layer after the decomposition of AgNWs.

The reasons responsible for the Ag whisker growth could be divided in two main categories: (1) intrinsic physical/chemical factors, and (2) e-beam induced factors. The first one can include: (a) thermal expansion of the coating versus that of the AgNWs and the substrate, and (b) diffusion of Ag in the porous coating structure and along its grain boundaries. The latter can be enhanced by such phenomena as: (a) local heating of the samples during SEM observation, (b) electric field induced migration of Ag. The mechanism of nanowhiskers growth is more detailed discussed in paper [IV].

As it can be seen from the above results the interaction between AgNW and titania layer does not always lead to thermal stability of AgNW like P. Ramasamy et al [6] have showed. In order to design this kind of layer structure it is important to systematically investigate interaction of different materials. The reported results clearly demonstrate that the combination of silicon substrate AgNW and thin titania layer can lead to the materials with non-conventional properties.

CONCLUSION

Elaboration of ceramic nanocomposites and design of functional coatings were conducted via sol-gel technique and described within this work. A complex approach was used combining synthesis, processing and advanced characterization techniques, which enabled to treat the considered problems and to cover different relevant aspects in a multi-discipline approach.

It was demonstrated, that sol-gel method enables to decrease synthesis temperatures and prepare homogeneous and pure multi component systems. In contrast to the conventional methods of synthesis of ceramic materials, sol-gel process reactants are mixed together at molecular level. The work covered preparation and investigation of several ceramic materials including TiC-ZrC, TiC/MWCNT, Al₂O₃ fibers and AgNW/TiO₂. As a part of my work, the activities also included development and construction of experimental set-up, which was used for *in situ* SEM mechanical characterization of individual one-dimensional nanostructures (1DNS). Nanoscale mechanical tests have contributed to better understanding of relations between size, geometry, composition and mechanical properties of individual 1DNS and helped to evaluate the applicability of certain nanostructures to serve as reinforcing phase or functional filler in the considered nanocomposites. The know-how and results acquired during this PhD thesis are the presumption for developing new CMC materials with novel properties using new synthesis and characterization methods. The flexibility of the sol-gel method for producing different ceramic materials like functional composites and surface coatings is shown in this work. Sol-gel method is a potential technique for the synthesis of Ultra High Temperature Ceramics homogeneous and pure multi-component materials by mixing the molecular precursor solutions and nanostructural fillers.

The main and novel results are summarized below:

- A synthesis method for TiC-ZrC nanocomposites was elaborated by combination of sol-gel and carbothermal reduction. The characterizations of the samples showed that the polymer precursor is suitable for preparation of TiC-ZrC, pure TiC and TiC/MWCNT composite. The XRD analysis of heat treated TiC-ZrC samples in argon and vacuum has shown that the carbothermal reduction of the binary solid carbide mixture (ZrC-TiC) polymeric precursor started in vacuum at lower temperature (1100 °C) than in argon environment. The ZrC-TiC binary compound is formed at 1600 °C in vacuum with a little amount of residual monoclinic ZrO₂ phase. Densification parameters of ZrC-TiC composite to single phase solid solution by spark plasma sintering were found out. The fracture of TiZrC₂ solid solution exhibits a mixed fracture mode with inter- and intra-granular cracking together with plastic grooving, which indicates the plasticity in microvolumes of the material.

- Mechanical characterization of sol-gel derived Al_2O_3 nanofibers before and after heating to $1400\text{ }^\circ\text{C}$ revealed significant enhancement of mechanical properties for annealed fibres, therefore proving the suitability of Al_2O_3 nanofibers for use in ceramic nanocomposites, where high processing temperatures are involved.
- Bending and fatigue tests of individual silver nanowires demonstrated suitability of AgNWs as a filler material for flexible transparent conductive ceramic coatings. Fatigue tests with several millions of cycles were performed. It was demonstrated that AgNWs have high fatigue resistance and can be bent elastically multiple times without failure.
- It was demonstrated that in addition to the increased thermal and chemical stability of AgNWs, combination of AgNWs and TiO_2 in a composite sol-gel derived coating can lead to formation and rapid growth of Ag nanowhiskers under electron beam irradiation. Optimal growth conditions were found and the factors of the growth were proposed.

SUMMARY IN ESTONIAN

Sool-geel tehnoloogia rakendamine keraamiliste nanokomposiitmaterjalide ja funktsionaalsete pinnakatete valmistamiseks

Nanokomposiitmaterjalide valmistamise üheks peamiseks probleemiks on armatuurina kasutatavate nanostruktuuride homogeenne segamine maatriksmaterjali, seejuures armatuuri kahjustamata. Traditsioonilises pulbertehnoloogias kasutatakse nanokomposiitide valmistamiseks peamiselt erinevaid jahvatusmeetodeid, mis võivad nanostruktuurset armatuuri vigastada ning isegi selle lagunemist põhjustada. Valmistamisprotsessis kahjustunud armatuuri tõttu võivad komposiidi omadused eeldatust kehvemad olla. Jahvatamisega võib kaasned ka mittesoovitavate lisandite sattumine „veskist” komposiiti, mille tulemusena loodava materjali omadused võivad muutuda. Lisaks piirab nanostruktuuride kasutamist armatuurina või funktsionaalsete osakestena keraamiliste komposiitmaterjalide valmistamiseks vajalik temperatuur kuna ka kuumus võib nanostruktuure kahjustada või hävitada.

Käesoleva töö eesmärgiks oli eelpool kirjeldatud probleeme vältides kontrollitud omadustega keraamiliste nanokomposiitmaterjalide ja funktsionaalsete katete väljatöötamine. Eesmärgi saavutamiseks läheneti probleemistikule komplekselt ehk kasutati sool-geel tehnoloogiat, materjalide töötlust kõrgetel temperatuuridel, täppis-karakteriseerimise meetodeid ja nano-osiste mehaaniliste omaduste karakteriseerimist.

Lähtudes sool-geel tehnoloogiast töötati välja nano-komposiitmaterjalide ja funktsionaalsete katete lähteainete sünteesimeetodid. Sool-geel meetodi kasutamise üheks peamiseks eeliseks eespoolmainitud alternatiivide ees on lähteainete segamine vedelikfaasis ehk molekulaarsel tasandil, mis tagab komposiitmaterjali homogeensuse. „Lisaks on kirjeldatud meetod äärmiselt paindlik võimaldades samast lähteainest väga erineva dimensionaalsusega objekte valmistada: pinnakatteid, komposiite, fiibreid ja pulbreid. Töö tulemusena leiti, et sool-geel meetodiga valmistatud lähteainete kasutamisel on võimalik oluliselt vähendada karbiidsete komposiitmaterjalide karbotermilise taandamise temperatuure. Analüüsi keraamiliste komposiitide TiC-ZrC, TiC/MWCNT ja Ag NW/TiO₂ sünteesi ja karakteristikuid. Lisanditena kasutatavate nanoosakeste mehaaniliste omaduste määramiseks töötati välja kõrglahutusega elektronmikroskoobi sisse paigutatav nanomanipulatsiooniseade. Erinevate koostistega nanostruktuuride karakteriseerimine võimaldab leida seoseid mehaaniliste omaduste ja osakeste suuruse ning nende geomeetrilise kuju vahel. See teave aitab valida sobivaid nanostruktuure komposiitmaterjalidessse funktsionaalse täitematerjalina või tugevdava armatuurina. Töös selgitati välja üksikute nanostruktuuride, Al₂O₃ fiibrite ja hõbedananotraatide, mis on potentsiaalsed kandidaadid armatuuriks või funktsionaalseks osakeseks komposiidis, mehaanilised omadused.

Töö peamised tulemused on:

- Töötati välja sool-geel meetodil ja karbotermilise taandamisega sünteesil põhinev meetod TiC-ZrC ja TiC/MWCNT komposiitide valmistamiseks. Karbiidide polümeerse lähteaine sünteesis sool-geel meetodil selgitati välja, et lähteaine karbotermiliseks taandamiseks vajaminev süsinikukogus lähteaines sõltub 1,4-dihüdroksübenseeni kogusest ja polükondensatsiooni-astmest lähteaines. Proovide iseloomustamine näitas, et sool-geel meetodil sünteesitud polümeerne lähteaine on sobilik TiC-ZrC, TiC and TiC/MWCNT valmistamiseks. Lisaks tehti kindlaks, et karbiidide polümeerse lähteaine karbotermiline taandamine algab vaakumis madalamal temperatuuril (1100 °C) kui argooni keskkonnas (1300 °C). Kahefaasiline TiC-ZrC, mis sisaldas vähesel määral ZrO₂-d, saadi peale ühetunnist karbotermilist taandamist 1600 °C vaakumis. Selgitati välja kahefaasilise TiC-ZrC paagutamisparameetrid ühefaasiliseks TiZrC₂ tahkeks lahuseks sädepaagutamise meetodil. TiZrC₂ murdepinnalt on näha, et materjal esineb graanulisest ja -välist pragunemist koos plastse pragunemisega, mis osutab antud materjali plastsusele mikroskaalas.
- Al₂O₃ nanokiudude mehaanilisel karakteriseerimisel näidati, et nanokiudude elastsusmoodul on väiksem võrreldes makroskaalas olevaga ja lisaks on neid võimalik painutada ka elastselt. Al₂O₃ nanokiudud pidasid vastu 1400 °C juures kuumutamisele ja toimus faasiüleminek kuubilisest γ – Al₂O₃ heksagoonalsesse α – Al₂O₃ faasi. Kuumutamata ja kuumutatud Al₂O₃ nanokiudude mehaaniline karakteriseerimine näitas kuumtöötamise mõju materjali mehaaniliste omadused paranemisele. Elastsusmoodul ja paindetugevus suurenesid keskmiselt peale kuumtöötlust ligi kaks korda. Mehaaniliste omaduste muutus tõestab nende sobilikkust kasutamaks kiude kõrgtemperatuursetes komposiitmaterialides armatuurina.
- Hõbenanotraatide (Ag NW) painutus- ja väsimuskatsed näitasid, et nanotraatide võrgustik on sobilik kasutamiseks painduvates ja tasapinnalistes-struktuurides. Väsimuskatse käigus selgus, et hõbenanotraadid peavad vastu miljon elastset painutust.
- Töötati välja meetod Ag NW võrgustiku katmiseks TiO₂ kilega. Lisaks Ag NW-de paranenud termilistele ja keemilistele omadustele näidati, et TiO₂ kilega kaetud Ag NW-del hakkavad elektronkiirguse mõjul kasvama „hõbenanovurrud”. Selgitati välja nanovurrude kasvu optimaalsed parameetrid ning kirjeldati võimalikke kasvumehhanisme. Viimaste uuringutega loodi eeldused kõnealuste struktuuride kasutamiseks sidusmaterjalides.

ACKNOWLEDGEMENTS

I am grateful to my scientific supervisors, Ants Lõhmus, Rünno Lõhmus and Irina Hussainova for involving and continuously supporting me during my PhD studies.

I am sincerely thankful to all of the co-authors for pleasant and effective teamwork. Special thanks goes to Sergei Vlassov for supervision in mechanical characterization at nanoscale and for constructive advice on the thesis, to Valter Reedo for supervising me in all chemistry connected activities and Leonid Dorogin for providing essential theoretical support, to Lauri Kollo for the help of the carbothermal reduction experiments and all other colleagues.

I am also grateful to Rando Saar for assistance with SEM, to Kathriin Utt for assistance with Raman spectroscopy, to Fredrik Punga and Madis Lobjakas for technical assistance.

I'm indescribably grateful to my family and Kadi Külasalu for their support.

I acknowledge the following agencies and foundations for financial support: Estonian Ministry of Education and Research (targeted projects IUT 19–29, IUT 2–25 and ETF 9281), the European Union through the European Regional Development Fund (Centre of Excellence “Mesosystems: Theory and Applications”, TK114), The Estonian Nanotechnology Competence Centre (EU29996), Archimedes Foundation project grant “Nano-Com” 3.2.1101.12-0010, “TRIBOFILM” 3.2.1101.12-0028 and “IRGLASS” 3.2.1101.12-0027.

REFERENCES

- [1] V. Viswanathan, T. Laha, K. Balani, A. Agarwal, and S. Seal, "Challenges and advances in nanocomposite processing techniques," *Mater. Sci. Eng. R Reports*, vol. 54, no. 5–6, pp. 121–285, Nov. 2006.
- [2] J. W. Martin, *Materials for Engineering, 3rd Edition*, 3rd ed. Cambridge: Woodhead Publishing, 2006, p. 256.
- [3] A. P. Ramirez, "Carbon nanotubes for science and technology," *Bell Labs Tech. J.*, vol. 10, no. 3, pp. 171–185, Nov. 2005.
- [4] A. Sommers, Q. Wang, X. Han, C. T'Joen, Y. Park, and A. Jacobi, "Ceramics and ceramic matrix composites for heat exchangers in advanced thermal systems—A review," *Appl. Therm. Eng.*, vol. 30, no. 11–12, pp. 1277–1291, Aug. 2010.
- [5] S. Vlassov, B. Polyakov, and L. Dorogin, "Shape Restoration Effect in Ag–SiO₂ Core–Shell Nanowires," *Nano ...*, 2014.
- [6] P. Ramasamy, D.-M. Seo, S.-H. Kim, and J. Kim, "Effects of TiO₂ shells on optical and thermal properties of silver nanowires," *J. Mater. Chem.*, vol. 22, no. 23, p. 11651, 2012.
- [7] S. Costacurta, P. Falcaro, S. Vezzù, M. Colasuonno, P. Scopece, E. Zanchetta, M. Guglielmi, and A. Patelli, "Fabrication of functional nanostructured coatings by a combined sol–gel and plasma-enhanced chemical vapour deposition method," *J. Sol-Gel Sci. Technol.*, vol. 60, no. 3, pp. 340–346, Sep. 2011.
- [8] S. Mathur, H. Shen, and J. Altmayer, "Nanostructured Functional Ceramic Coatings By Molecule-Based Chemical Vapor Deposition," *Rev. od Adv. Mater. Science*, vol. 15, pp. 16–23, 2007.
- [9] M. R. Falvo and R. Superfine, "Mechanics and friction at the nanometer scale," pp. 237–248, 2000.
- [10] S. M. El-Sheikh, Z. I. Zaki, and Y. M. Z. Ahmed, "In situ synthesis of ZrC/SiC nanocomposite via carbothermic reduction of binary xerogel," *J. Alloys Compd.*, vol. 613, pp. 379–386, Nov. 2014.
- [11] C. Yan, R. Liu, Y. Cao, C. Zhang, and D. Zhang, "Ablation behavior and mechanism of C/ZrC, C/ZrC–SiC and C/SiC composites fabricated by polymer infiltration and pyrolysis process," *Corros. Sci.*, vol. 86, pp. 131–141, Sep. 2014.
- [12] V. Singh, R. Diaz, K. Balani, A. Agarwal, and S. Seal, "Chromium carbide–CNT nanocomposites with enhanced mechanical properties," *Acta Mater.*, vol. 57, no. 2, pp. 335–344, Jan. 2009.
- [13] S. E. Landwehr, G. E. Hilmas, W. G. Fahrenholtz, I. G. Talmy, and S. G. DiPietro, "Microstructure and mechanical characterization of ZrC–Mo cermets produced by hot isostatic pressing," *Mater. Sci. Eng. A*, vol. 497, no. 1–2, pp. 79–86, Dec. 2008.
- [14] I. Krenkel, "Carbon fibre reinforced silicon carbide composites (C/SiC, C/C–SiC)," *Handb. Ceram. Compos.*, pp. 117–148, 2005.
- [15] H. PERSON, *Handbook of refractory carbides and nitrides*. Noyes Publications, 1996.
- [16] S. T. Oyama, Ed., *The Chemistry of Transition Metal Carbides and Nitrides*, First edit. Blackie Academic & Professional, 1996.

- [17] D. Vallauri, I. A. Adrian, and A. Chrysanthou, "TiC–TiB₂ composites: A review of phase relationships, processing and properties," *J. Eur. ...*, vol. 28, pp. 1697–1713, 2008.
- [18] C. Giordano and M. Antonietti, "Synthesis of crystalline metal nitride and metal carbide nanostructures by sol–gel chemistry," *Nano Today*, vol. 6, no. 4, pp. 366–380, Aug. 2011.
- [19] R. B. Acicbe and G. Goller, "Densification behavior and mechanical properties of spark plasma-sintered ZrC–TiC and ZrC–TiC–CNT composites," *J. Mater. Sci.*, vol. 48, no. 6, pp. 2388–2393, Nov. 2012.
- [20] M. J. Gasch, D. T. Ellerby, and S. M. Johnson, "Ultra High Temperature Ceramic Composites," in *Handbook of Ceramic Composites*, 2005, pp. 197–224.
- [21] D. J. Ham and J. S. Lee, "Transition Metal Carbides and Nitrides as Electrode Materials for Low Temperature Fuel Cells," *Energies*, vol. 2, no. 4, pp. 873–899, Oct. 2009.
- [22] J. Zhong, Y. Peng, M. Zhou, J. Zhao, S. Liang, H. Wang, and Y.-B. Cheng, "Facile synthesis of nanoporous TiC–SiC–C composites as a novel counter-electrode for dye sensitized solar cells," *Microporous Mesoporous Mater.*, vol. 190, pp. 309–315, May 2014.
- [23] X. Yuan, L. Cheng, L. Kong, X. Yin, and L. Zhang, "Preparation of titanium carbide nanowires for application in electromagnetic wave absorption," *J. Alloys Compd.*, vol. 596, no. 3, pp. 132–139, May 2014.
- [24] Y. Katoh, G. Vasudevamurthy, T. Nozawa, and L. L. Snead, "Properties of zirconium carbide for nuclear fuel applications," *J. Nucl. Mater.*, vol. 441, no. 1–3, pp. 718–742, Oct. 2013.
- [25] D. L. Yung, L. Kollo, I. Hussainova, and A. Žikin, "Reactive Sintering of ZrC–TiC Composites," *Key Eng. Mater.*, vol. 527, pp. 20–25, Nov. 2012.
- [26] S. E. Landwehr, G. E. Hilmas, W. G. Fahrenholtz, and I. G. Talmy, "Processing of ZrC–Mo Cermets for High-Temperature Applications, Part I: Chemical Interactions in the ZrC–Mo System," *J. Am. Ceram. Soc.*, vol. 90, no. 7, pp. 1998–2002, Jul. 2007.
- [27] T. Suzuki, H. Matsumoto, N. Nomura, and S. Hanada, "Microstructures and fracture toughness of directionally solidified Mo–ZrC eutectic composites," *Sci. Technol. Adv. Mater.*, vol. 3, no. 2, pp. 137–143, Mar. 2002.
- [28] I. Hussainova, M. Antonov, and N. Voltsihhin, "Assessment of zirconia doped hardmetals as tribomaterials," *Wear*, vol. 271, no. 9–10, pp. 1909–1915, Jul. 2011.
- [29] I. Hussainova, N. Volt, E. Cura, and S. Hannula, "Densification and characterization of spark plasma sintered ZrC – ZrO₂ composites," vol. 597, pp. 75–81, 2014.
- [30] S. M. Kats, S. S. Ordan'yan, and V. I. Unrod, "Compressive creep of alloys of the ZrC–ZrB₂ and TiC–TiB₂ systems," *Sov. Powder Metall. Met. Ceram.*, vol. 20, no. 12, pp. 886–890, Dec. 1981.
- [31] F. Wakai, N. Kondo, and Y. Shinoda, "Ceramics superplasticity," vol. 4, no. 1999, pp. 461–465, 2000.
- [32] O. Adjaoud, G. Steinle-Neumann, B. Burton, and a. van de Walle, "First-principles phase diagram calculations for the HfC–TiC, ZrC–TiC, and HfC–ZrC solid solutions," *Phys. Rev. B*, vol. 80, no. 13, p. 134112, Oct. 2009.

- [33] V. I. Ivashchenko, P. E. a Turchi, and V. I. Shevchenko, "First-principles study of elastic and stability properties of ZrC-ZrN and ZrC-TiC alloys.," *J. Phys. Condens. Matter*, vol. 21, no. 39, p. 395503, Sep. 2009.
- [34] S. Liu, W. Hu, J. Xiang, F. Wen, B. Xu, D. Yu, J. He, Y. Tian, and Z. Liu, "Mechanical properties of nanocrystalline TiC-ZrC solid solutions fabricated by spark plasma sintering," *Ceram. Int.*, vol. 40, no. 7, pp. 10517–10522, Aug. 2014.
- [35] C. Mroz, "Processing and Properties of Microcomposite TiZrC and TiZrB2 Materials," in *Proceedings of the 17th Annual Conference on Composites and Advanced Ceramic Materials: Ceramic Engineering and Science Proceedings*, John Wiley & Sons, Inc., 1993, pp. 725–735.
- [36] L. Berger, W. Gruner, E. Langholf, and S. Stolle, "On the mechanism of carbothermal reduction processes of TiO₂ and ZrO₂," *Int. J. Refract. Met. Hard Mater.*, vol. 17, no. 1–3, pp. 235–243, May 1999.
- [37] W. SEN, B. XU, B. YANG, H. SUN, J. SONG, H. WAN, and Y. DAI, "Preparation of TiC powders by carbothermal reduction method in vacuum," *Trans. Nonferrous Met. Soc. China*, vol. 21, no. 1, pp. 185–190, Jan. 2011.
- [38] N. Chandra, M. Sharma, D. K. Singh, and S. S. Amritphale, "Synthesis of nano-TiC powder using titanium gel precursor and carbon particles," *Mater. Lett.*, vol. 63, no. 12, pp. 1051–1053, May 2009.
- [39] J. Li, Z. Y. Fu, W. M. Wang, H. Wang, S. H. Lee, and K. Niihara, "Preparation of ZrC by self-propagating high-temperature synthesis," *Ceram. Int.*, vol. 36, no. 5, pp. 1681–1686, Jul. 2010.
- [40] M. S. Kovalchenko, "Pressure sintering kinetics of tungsten and titanium carbides," *Int. J. Refract. Met. Hard Mater.*, vol. 39, pp. 32–37, Jul. 2013.
- [41] B. Núñez-González, A. L. Ortiz, F. Guiberteau, and M. Nygren, "Spark-plasma-sintering kinetics of ZrC-SiC powder mixtures subjected to high-energy co-ball-milling," *Ceram. Int.*, vol. 39, no. 8, pp. 9691–9697, Dec. 2013.
- [42] S.-K. Sun, G.-J. Zhang, W.-W. Wu, J.-X. Liu, T. Suzuki, and Y. Sakka, "Reactive spark plasma sintering of ZrC and HfC ceramics with fine microstructures," *Scr. Mater.*, vol. 69, no. 2, pp. 139–142, Jul. 2013.
- [43] I. Hasegawa, Y. Fukuda, and M. Kajiwara, "Inorganic-organic hybrid route to synthesis of ZrC and Si-Zr-C fibres," *Ceram. Int.*, vol. 25, no. 6, pp. 523–527, Aug. 1999.
- [44] M. Narisawa, S. Kida, T. Simoo, K. Okamura, and Y. Kurachi, "Synthesis of TiC-C fiber from titanium isopropoxide treated phenolic resin fiber," *J. Sol-Gel Sci. Technol.*, vol. 4, no. 1, pp. 31–35, 1995.
- [45] X. M. Cui, Y. S. Nam, J. Y. Lee, and W. H. Park, "Fabrication of zirconium carbide (ZrC) ultra-thin fibers by electrospinning," *Mater. Lett.*, vol. 62, no. 12–13, pp. 1961–1964, Apr. 2008.
- [46] F. Piazza, G. Morell, J. Beltran-Huarac, G. Paredes, M. Ahmadi, and M. Guinel, "Carbon nanotubes coated with diamond nanocrystals and silicon carbide by hot-filament chemical vapor deposition below 200°C substrate temperature," *Carbon N. Y.*, vol. 75, pp. 113–123, Aug. 2014.
- [47] C. Verdon, O. Szwedek, S. Jacques, a. Allemand, and Y. Le Petitcorps, "Hafnium and silicon carbide multilayer coatings for the protection of carbon composites," *Surf. Coatings Technol.*, vol. 230, pp. 124–129, Sep. 2013.
- [48] D. Wolfe, J. Singh, and K. Narasimhan, "Synthesis and characterization of multilayered TiC/TiB₂ coatings deposited by ion beam assisted, electron

- beam–physical vapor deposition (EB–PVD),” *Surf. Coatings Technol.*, vol. 165, no. 1, pp. 8–25, Feb. 2003.
- [49] M. Balzer and M. Fenker, “Three-dimensional thickness and property distribution of TiC films deposited by DC magnetron sputtering and HIPIMS,” *Surf. Coatings Technol.*, vol. 250, pp. 37–43, Jul. 2014.
- [50] a. Isalgue, J. Fernandez, N. Cinca, M. Villa, and J. M. Guilemany, “Mechanical and nanoindentation behavior of TiC–NiTi thermal spray coatings,” *J. Alloys Compd.*, vol. 577, pp. S277–S281, Nov. 2013.
- [51] M. Ali and P. Basu, “Mechanochemical synthesis of nano-structured TiC from TiO₂ powders,” *J. Alloys Compd.*, vol. 500, no. 2, pp. 220–223, Jun. 2010.
- [52] M. Umalas, V. Reedo, A. Löhmus, I. Hussainova, and K. Juhani, “Synthesis of ZrC–TiC Blend by Novel Combination of Sol-Gel Method and Carbothermal Reduction,” *Key Eng. Mater.*, vol. 527, pp. 62–67, Nov. 2012.
- [53] A. M. Shul’pekov and G. V. Lyamina, “Electrical and thermomechanical properties of materials based on nonstoichiometric titanium carbide prepared by self-propagating high-temperature synthesis,” *Inorg. Mater.*, vol. 47, no. 7, pp. 722–727, Jun. 2011.
- [54] I. P. Borovinskaya, T. I. Ignat’eva, V. I. Vershinnikov, O. M. Miloserdova, and V. N. Semenova, “Self-propagating high-temperature synthesis of ultrafine and nanosized WC and TiC powders,” *Powder Metall. Met. Ceram.*, vol. 47, no. 9–10, pp. 505–511, Jan. 2009.
- [55] D. Zhao, H. Hu, C. Zhang, Y. Zhang, and J. Wang, “A simple way to prepare precursors for zirconium carbide,” *J. Mater. Sci.*, vol. 45, no. 23, pp. 6401–6405, Jul. 2010.
- [56] H. Zhang, F. Li, Q. Jia, and G. Ye, “Preparation of titanium carbide powders by sol–gel and microwave carbothermal reduction methods at low temperature,” *J. Sol-Gel Sci. Technol.*, vol. 46, no. 2, pp. 217–222, Feb. 2008.
- [57] H. Preiss, L. Berger, and D. Schultze, “Studies on the carbothermal preparation of titanium carbide from different gel precursors,” *J. Eur. Ceram. Soc.*, vol. 19, no. 2, pp. 195–206, Feb. 1999.
- [58] X. Y. Tao, W. F. Qiu, H. Li, T. Zhao, and X. Y. Wei, “New route to synthesize preceramic polymers for zirconium carbide,” *Chinese Chem. Lett.*, vol. 23, no. 9, pp. 1075–1078, Sep. 2012.
- [59] H. Preiss, E. Schierhorn, and K. W. Brzezinka, “Synthesis of Polymeric Titanium and Zirconium Precursors and Preparation of Carbide Fibres and Films,” *J. Mater. Sci.*, vol. 33, pp. 4697–4706, 1998.
- [60] S. Sōmiya, F. Aldinger, N. Claussen, R. M. Spriggs, K. Uchino, K. Koumoto, M. Kaneno, L. C. De Jonghe, and M. N. Rahaman, “Handbook of Advanced Ceramics,” in *Handbook of Advanced Ceramics*, vol. I, 2003, pp. 187–264.
- [61] S. E. Landwehr, G. E. Hilmas, W. G. Fahrenholtz, I. G. Talmy, and H. Wang, “Thermal properties and thermal shock resistance of liquid phase sintered ZrC–Mo cermets,” *Mater. Chem. Phys.*, vol. 115, no. 2–3, pp. 690–695, Jun. 2009.
- [62] J. M. Córdoba, E. Chicardi, and F. J. Gotor, “Liquid-phase sintering of Ti(C,N)-based cermets. The effects of binder nature and content on the solubility and wettability of hard ceramic phases,” *J. Alloys Compd.*, vol. 559, pp. 34–38, May 2013.
- [63] C. Heiligers, C. J. Pretorius, and J. H. Neethling, “Interdiffusion of hafnium carbide and titanium carbide during hot-pressing,” *Int. J. Refract. Met. Hard Mater.*, vol. 31, pp. 51–55, Mar. 2012.

- [64] X.-G. Wang, J.-X. Liu, Y.-M. Kan, and G.-J. Zhang, "Effect of solid solution formation on densification of hot-pressed ZrC ceramics with MC (M=V, Nb, and Ta) additions," *J. Eur. Ceram. Soc.*, vol. 32, no. 8, pp. 1795–1802, Jul. 2012.
- [65] B. Ertuğ, *Sintering Applications*. InTech, 2013.
- [66] J. Cho, A. R. Boccaccini, and M. S. P. Shaffer, "Ceramic matrix composites containing carbon nanotubes," *J. Mater. Sci.*, vol. 44, no. 8, pp. 1934–1951, Feb. 2009.
- [67] E. Zapata-Solvas, D. Gómez-García, and a. Domínguez-Rodríguez, "Towards physical properties tailoring of carbon nanotubes-reinforced ceramic matrix composites," *J. Eur. Ceram. Soc.*, vol. 32, no. 12, pp. 3001–3020, Sep. 2012.
- [68] A. Licciulli, V. Contaldi, S. K. Padmanabhan, A. Balakrishnan, C. Siligardi, and D. Diso, "Influence of glass phase on Al₂O₃ fiber-reinforced Al₂O₃ composites processed by slip casting," *J. Eur. Ceram. Soc.*, vol. 31, no. 3, pp. 385–389, Mar. 2011.
- [69] V. O. Almeida, N. M. Balzaretto, T. M. H. Costa, G. B. Machado, and M. R. Gallas, "Surfactants for CNTs dispersion in zirconia-based ceramic matrix by sol-gel method," *J. Sol-Gel Sci. Technol.*, vol. 65, no. 2, pp. 143–149, Nov. 2012.
- [70] A. Kim, S. Lim, D.-H. Peck, S.-K. Kim, B. Lee, and D. Jung, "Preparation and Characteristics of SiO_x Coated Carbon Nanotubes with High Surface Area," *Nanomaterials*, vol. 2, no. 4, pp. 206–216, Jun. 2012.
- [71] X. Wu, J. Qiu, W. Zhang, L. Zang, E. Sakai, and P. Liu, "Synthesizing multi-walled carbon nanotube-polymethyl methacrylate conductive composites and poly(lactic acid) based composites," *Polym. Compos.*, p. n/a–n/a, Aug. 2014.
- [72] Q. Y. Tang, I. Shafiq, Y. C. Chan, N. B. Wong, and R. Cheung, "Study of the Dispersion and Electrical Properties of Carbon Nanotubes Treated by Surfactants in Dimethylacetamide," *J. Nanosci. Nanotechnol.*, vol. 10, no. 8, pp. 4967–4974, Aug. 2010.
- [73] C. B. Mo, S. I. Cha, K. T. Kim, K. H. Lee, and S. H. Hong, "Fabrication of carbon nanotube reinforced alumina matrix nanocomposite by sol-gel process," *Mater. Sci. Eng. A*, vol. 395, no. 1–2, pp. 124–128, Mar. 2005.
- [74] S. R. Inbaraj, R. M. Francis, N. V. Jaya, and A. Kumar, "Processing and properties of sol gel derived alumina-carbon nano tube composites," *Ceram. Int.*, vol. 38, no. 5, pp. 4065–4074, Jul. 2012.
- [75] C. Zhang, L. Gao, and Y. Chen, "Fabrication of ceramic oxide-coated SWNT composites by sol-gel process with a polymer glue," *J. Nanoparticle Res.*, vol. 13, no. 9, pp. 3731–3740, Feb. 2011.
- [76] B. N. Dudkin, a. Y. Bugaeva, G. G. Zainullin, and V. N. Filippov, "Corundum/lanthanum hexaaluminate/alumina nanofiber ceramic composite," *Inorg. Mater.*, vol. 46, no. 4, pp. 445–448, Apr. 2010.
- [77] Y. Bautista, J. Gonzalez, J. Gilabert, M. J. Ibañez, and V. Sanz, "Correlation between the wear resistance, and the scratch resistance, for nanocomposite coatings," *Prog. Org. Coatings*, vol. 70, no. 4, pp. 178–185, Apr. 2011.
- [78] I. A. Podchernyaeva, D. V. Yurechko, and V. M. Panashenko, "SOME TRENDS IN THE DEVELOPMENT OF WEAR-RESISTANT FUNCTIONAL COATINGS," vol. 52, no. 3, pp. 176–188, 2013.
- [79] D. Martínez-Martínez, O. Kubová, and M.-P. Delplancke-Ogletree, "Structural and Mechanical Study of Nanocomposite Ti-Zr-C-H Coatings Prepared by

- Reactive Magnetron Sputtering,” *Plasma Process. Polym.*, vol. 6, no. S1, pp. S554–S559, Jun. 2009.
- [80] R. Wang, K. Hashimoto, A. Fujishima, M. Chikuni, E. Kojima, A. Kitamura, M. Shimohigoshi, and T. Watanabe, “Light-induced amphiphilic surfaces,” *Nature*, vol. 388, pp. 431–432, 1997.
- [81] K. Nakata and A. Fujishima, “TiO₂ photocatalysis: Design and applications,” *J. Photochem. Photobiol. C Photochem. Rev.*, vol. 13, no. 3, pp. 169–189, Sep. 2012.
- [82] S. El-Sherbiny, F. Morsy, M. Samir, and O. a. Fouad, “Synthesis, characterization and application of TiO₂ nanopowders as special paper coating pigment,” *Appl. Nanosci.*, vol. 4, no. 3, pp. 305–313, Mar. 2013.
- [83] M. H. Ahmed, T. E. Keyes, J. a. Byrne, C. W. Blackledge, and J. W. Hamilton, “Adsorption and photocatalytic degradation of human serum albumin on TiO₂ and Ag–TiO₂ films,” *J. Photochem. Photobiol. A Chem.*, vol. 222, no. 1, pp. 123–131, Jul. 2011.
- [84] A. Kim, Y. Won, K. Woo, C. Kim, J. Moon, and K. I. M. E. T. Al, “Highly Transparent Low Resistance ZnO / Ag Nanowire / ZnO Composite Electrode for Thin Film Solar Cells,” no. 2, pp. 1081–1091, 2013.
- [85] R. Pärna, U. Joost, E. Nõmmiste, T. Käämbre, A. Kikas, I. Kuusik, M. Hirsimäki, I. Kink, and V. Kisand, “Effect of cobalt doping and annealing on properties of titania thin films prepared by sol–gel process,” *Appl. Surf. Sci.*, vol. 257, no. 15, pp. 6897–6907, May 2011.
- [86] O. Akhavan, “Lasting antibacterial activities of Ag–TiO₂/Ag/a–TiO₂ nano-composite thin film photocatalysts under solar light irradiation,” *J. Colloid Interface Sci.*, vol. 336, no. 1, pp. 117–24, Aug. 2009.
- [87] C.-H. Chung, T.-B. Song, B. Bob, R. Zhu, and Y. Yang, “Solution-processed flexible transparent conductors composed of silver nanowire networks embedded in indium tin oxide nanoparticle matrices,” *Nano Res.*, vol. 5, no. 11, pp. 805–814, Oct. 2012.
- [88] H. H. Khaligh and I. a Goldthorpe, “Failure of silver nanowire transparent electrodes under current flow,” *Nanoscale Res. Lett.*, vol. 8, no. 1, p. 235, Jan. 2013.
- [89] S. Vlassov, B. Polyakov, L. M. Dorogin, M. Antsov, M. Mets, M. Umalas, R. Saar, R. Löhmus, and I. Kink, “Elasticity and yield strength of pentagonal silver nanowires: In situ bending tests,” *Mater. Chem. Phys.*, vol. 143, no. 3, pp. 1026–1031, Feb. 2014.
- [90] K. Zilberberg, F. Gasse, R. Pagui, A. Polywka, A. Behrendt, S. Trost, R. Heiderhoff, P. Görrn, and T. Riedl, “Highly Robust Indium-Free Transparent Conductive Electrodes Based on Composites of Silver Nanowires and Conductive Metal Oxides,” *Adv. Funct. Mater.*, vol. 24, no. 12, pp. 1671–1678, Mar. 2014.
- [91] B. Polyakov, L. M. Dorogin, S. Vlassov, I. Kink, a. Lohmus, a. E. Romanov, and R. Lohmus, “Real-time measurements of sliding friction and elastic properties of ZnO nanowires inside a scanning electron microscope,” *Solid State Commun.*, vol. 151, no. 18, pp. 1244–1247, Sep. 2011.
- [92] B. Polyakov, M. Antsov, S. Vlassov, L. M. Dorogin, M. Vahtrus, R. Zabels, S. Lange, and R. Löhmus, “Mechanical properties of sol–gel derived SiO₂ nanotubes,” *Beilstein J. Nanotechnol.*, vol. 5, pp. 1808–1814, Oct. 2014.

- [93] Z. L. Wang, R. P. Gao, P. Poncharal, W. A. De Heer, Z. R. Dai, and Z. W. Pan, "Mechanical and electrostatic properties of carbon nanotubes and nanowires," pp. 3–10, 2001.
- [94] Z. Zhao, X. Shen, H. Yao, J. Wang, J. Chen, and Z. Li, "Alumina nanofibers obtained via electrospinning of pseudo-boehmite sol/PVP solution," *J. Sol-Gel Sci. Technol.*, vol. 70, no. 1, pp. 72–80, Jan. 2014.
- [95] P. Zhang, D. Chen, and X. Jiao, "Fabrication of Flexible α -Alumina Fibers Composed of Nanosheets," *Eur. J. Inorg. Chem.*, vol. 2012, no. 26, pp. 4167–4173, Sep. 2012.
- [96] E. W. Wong, P. E. Sheehan, and C. M. Lieber, "Nanobeam Mechanics: Elasticity, Strength, and Toughness of Nanorods and Nanotubes," vol. 277, no. September, pp. 1971–1975, 1997.
- [97] S. Vlassov, B. Polyakov, L. M. Dorogin, A. Löhmus, A. E. Romanov, I. Kink, E. Gnecco, and R. Löhmus, "Real-time manipulation of gold nanoparticles inside a scanning electron microscope," *Solid State Commun.*, vol. 151, no. 9, pp. 688–692, May 2011.
- [98] Y. Zhu, Q. Qin, F. Xu, F. Fan, Y. Ding, T. Zhang, B. J. Wiley, and Z. L. Wang, "Size effects on elasticity, yielding, and fracture of silver nanowires: In situ experiments," *Phys. Rev. B*, vol. 85, no. 4, p. 045443, Jan. 2012.
- [99] P. G. Allison, R. D. Moser, J. P. Schirer, R. . Martens, J. B. Jordon, and M. Q. Chandler, "In-situ nanomechanical studies of deformation and damage mechanisms in nanocomposites monitored using scanning electron microscopy," *Mater. Lett.*, vol. 131, pp. 313–316, Sep. 2014.
- [100] C.-C. Röhlig, M. Niebelschütz, K. Brueckner, K. Tonisch, O. Ambacher, and V. Cimalla, "Elastic properties of nanowires," *Phys. Status Solidi*, vol. 247, no. 10, pp. 2557–2570, Sep. 2010.
- [101] K. Zheng, C. Wang, Y.-Q. Cheng, Y. Yue, X. Han, Z. Zhang, Z. Shan, S. X. Mao, M. Ye, Y. Yin, and E. Ma, "Electron-beam-assisted superplastic shaping of nanoscale amorphous silica," *Nat. Commun.*, vol. 1, no. 3, p. 24, Jan. 2010.
- [102] B. Polyakov, L. Dorogin, S. Vlassov, I. Kink, and R. Löhmus, "Tribological Aspects of In Situ Manipulation of Nanostructures Inside Scanning Electron Microscope," in *Fundamentals of Friction and Wear on the Nanoscale SE - 18*, E. Gnecco and E. Meyer, Eds. Springer International Publishing, 2015, pp. 395–426.
- [103] a. D. Pomogailo, "Polymer Sol-Gel Synthesis of Hybrid Nanocomposites," *Colloid J.*, vol. 67, no. 6, pp. 658–677, Nov. 2005.
- [104] B. Gawel, K. Gawel, and G. Øye, "Sol-Gel Synthesis of Non-Silica Monolithic Materials," *Materials (Basel)*, vol. 3, no. 4, pp. 2815–2833, Apr. 2010.
- [105] "Sol-Gel Processing of Ceramics and Glass," *BCC Research*, 2012. [Online]. Available: <http://www.bccresearch.com/market-research/advanced-materials/sol-gel-processing-ceramics-glass-avm016f.html> 2015.
- [106] S. Sakka, "Handbook of sol-gel science and technology, vol. I–III," 2005.
- [107] R. Pérez-Hernández, D. Mendoza-Anaya, M. E. Fernández, and a. Gómez-Cortés, "Synthesis of mixed ZrO₂–TiO₂ oxides by sol-gel: Microstructural characterization and infrared spectroscopy studies of NO_x," *J. Mol. Catal. A Chem.*, vol. 281, no. 1–2, pp. 200–206, Feb. 2008.
- [108] A. Kitiyanan, S. Ngamsinlapasathian, S. Pavasupree, and S. Yoshikawa, "The preparation and characterization of nanostructured TiO₂–ZrO₂ mixed oxide

- electrode for efficient dye-sensitized solar cells,” *J. Solid State Chem.*, vol. 178, no. 4, pp. 1044–1048, Apr. 2005.
- [109] L. Klein, “Sol-gel technology for thin films, fibers, preforms, electronics, and specialty shapes,” p. 428, 1988.
- [110] J. Livage, M. Henry, and C. Sanchez, “Sol-gel chemistry of transition metal oxides,” *Prog. Solid State Chem.*, vol. 18, no. 4, pp. 259–341, Jan. 1988.
- [111] H. Jiang and C. Blouin, “Insertions and the emergence of novel protein structure: a structure-based phylogenetic study of insertions,” *BMC Bioinformatics*, vol. 8, p. 444, Jan. 2007.
- [112] M. T. Harris, A. Singhal, J. E. E. L. Look, J. R. Smith-kristensen, J. A. R. S. Lin, and L. M. Toth, “FTIR Spectroscopy , SAXS and Electrical Conductivity Studies of the Hydrolysis and Condensation of Zirconium and Titanium Alkoxides,” vol. 4147, 1997.
- [113] V. G. Kessler, G. I. Spijksma, G. a. Seisenbaeva, S. Håkansson, D. H. a. Blank, and H. J. M. Bouwmeester, “New insight in the role of modifying ligands in the sol-gel processing of metal alkoxide precursors: A possibility to approach new classes of materials,” *J. Sol-Gel Sci. Technol.*, vol. 40, no. 2–3, pp. 163–179, Jul. 2006.
- [114] B. E. Yoldas, “Hydrolysis of titanium alkoxide and effects of hydrolytic polycondensation parameters,” *J. Mater. Sci.*, vol. 21, no. 3, pp. 1087–1092, Mar. 1986.
- [115] A. Araoyinbo, M. N. Ahmad Fauz, S. Sreekantan, and A. Aziz, “Preparation and Characterization of Thin Film TiO₂ Dip Coated on Non-Conductive Substrate Prepared from Tetraethyl Orthotitanate Precursor,” *Asian J. Appl. Sci.*, vol. 3, no. 1, pp. 35–43, Jan. 2010.
- [116] V. G. Kessler, “The chemistry behind the sol–gel synthesis of complex oxide nanoparticles for bio-imaging applications,” *J. Sol-Gel Sci. Technol.*, vol. 51, no. 3, pp. 264–271, Mar. 2009.
- [117] G. Oskam, “Metal oxide nanoparticles: synthesis, characterization and application,” *J. Sol-Gel Sci. Technol.*, vol. 37, no. 3, pp. 161–164, Feb. 2006.
- [118] C. J. Brinker and G. W. Scherer, *Sol-gel science: the physics and chemistry of sol-gel processing*, vol. 8. 1990, p. 908.
- [119] J. M. Nedelec, “Sol-Gel Processing of Nanostructured Inorganic Scintillating Materials,” *J. Nanomater.*, vol. 2007, pp. 1–8, 2007.
- [120] J. Zhong, S. Liang, J. Zhao, W. D. Wu, W. Liu, H. Wang, X. D. Chen, and Y.-B. Cheng, “Formation of novel mesoporous TiC microspheres through a sol–gel and carbothermal reduction process,” *J. Eur. Ceram. Soc.*, vol. 32, no. 12, pp. 3407–3414, Sep. 2012.
- [121] M. Dollé, D. Gosset, C. Bogicevic, F. Karolak, D. Simeone, and G. Baldinozzi, “Synthesis of nanosized zirconium carbide by a sol–gel route,” *J. Eur. Ceram. Soc.*, vol. 27, no. 4, pp. 2061–2067, Jan. 2007.
- [122] M. D. Sacks, C.-A. Wang, Z. Yang, and A. Jain, “Carbothermal reduction synthesis of nanocrystalline zirconium carbide and hafnium carbide powders using solution-derived precursors,” *J. Mater. Sci.*, vol. 39, no. 19, pp. 6057–6066, Oct. 2004.
- [123] M. Alzamani, A. Shokuhfar, E. Eghdam, and S. Mastali, “Influence of catalyst on structural and morphological properties of TiO₂ nanostructured films prepared by sol–gel on glass,” *Prog. Nat. Sci. Mater. Int.*, vol. 23, no. 1, pp. 77–84, Feb. 2013.

- [124] S. Sahni, S. B. Reddy, and B. S. Murty, "Influence of process parameters on the synthesis of nano-titania by sol-gel route," *Mater. Sci. Eng. A*, vol. 452–453, pp. 758–762, Apr. 2007.
- [125] V. G. Sevastyanov, E. P. Simonenko, N. a. Ignatov, Y. S. Ezhov, N. P. Simonenko, and N. T. Kuznetsov, "Low-temperature synthesis of nanodispersed titanium, zirconium, and hafnium carbides," *Russ. J. Inorg. Chem.*, vol. 56, no. 5, pp. 661–672, Jun. 2011.
- [126] Y. Yan, Z. Huang, X. Liu, and D. Jiang, "Carbothermal synthesis of ultra-fine zirconium carbide powders using inorganic precursors via sol-gel method," *J. Sol-Gel Sci. Technol.*, vol. 44, no. 1, pp. 81–85, Aug. 2007.
- [127] C. R. Rambo, J. Cao, O. Rusina, and H. Sieber, "Manufacturing of biomorphic (Si,Ti,Zr)-carbide ceramics by sol-gel processing," *Carbon N. Y.*, vol. 43, no. 6, pp. 1174–1183, May 2005.
- [128] M. A. Majeed Khan, S. Kumar, M. Ahamed, S. a Alrokayan, and M. S. Alsalhi, "Structural and thermal studies of silver nanoparticles and electrical transport study of their thin films.," *Nanoscale Res. Lett.*, vol. 6, no. 1, p. 434, Jan. 2011.
- [129] S. Timoshenko and J. N. Goodier, *Theory of Elasticity*. 1951.
- [130] L. M. Dorogin, S. Vlassov, B. Polyakov, M. Antsov, R. Löhmus, I. Kink, and A. E. Romanov, "Real-time manipulation of ZnO nanowires on a flat surface employed for tribological measurements: Experimental methods and modeling," *Phys. status solidi*, vol. 250, no. 2, pp. 305–317, Feb. 2013.
- [131] D. Smith, V. Holmberg, and B. Korgel, "Flexible germanium nanowires: ideal strength, room temperature plasticity, and bendable semiconductor fabric," *ACS Nano*, vol. 4, no. 4, pp. 2356–62, Apr. 2010.
- [132] F. Perrin, V. Nguyen, and J. Vernet, "FT-IR Spectroscopy of acid-modified titanium alkoxides: investigations on the nature of carboxylate coordination and degree of complexation," *J. sol-gel Sci. ...*, pp. 205–215, 2003.
- [133] G. Asano, T. Satake, K. Ohtsuki, and H. Funakubo, "In situ FTIR investigation of the effect of gas-phase reaction on the deposition of Pb(Zr,Ti)O₃ films by MOCVD," *Thin Solid Films*, vol. 498, no. 1–2, pp. 277–281, Mar. 2006.
- [134] B. H. Lohse, A. Calka, and D. Wexler, "Raman spectroscopy sheds new light on TiC formation during the controlled milling of titanium and carbon," *J. Alloys Compd.*, vol. 434–435, pp. 405–409, May 2007.
- [135] J. Macan, a. Gajović, and H. Ivanković, "Porous zirconium titanate ceramics synthesized by sol-gel process," *J. Eur. Ceram. Soc.*, vol. 29, no. 4, pp. 691–696, Mar. 2009.
- [136] B. M. Reddy, P. M. Sreekanth, Y. Yamada, Q. Xu, and T. Kobayashi, "Surface characterization of sulfate, molybdate, and tungstate promoted TiO₂-ZrO₂ solid acid catalysts by XPS and other techniques," *Appl. Catal. A Gen.*, vol. 228, no. 1–2, pp. 269–278, Mar. 2002.
- [137] S.-H. Yeon, R. Patel, J.-K. Koh, S.-H. Ahn, and J.-H. Kim, "Preparation of Porous TiO₂ Thin Films by Poly(vinyl chloride)-graft-poly(N-vinyl pyrrolidone) and Their Applications to Dye-sensitized Solar Cells," *J. Korean Electrochem. Soc.*, vol. 14, no. 2, pp. 83–91, May 2011.
- [138] C. Jing, X. Xu, and J. Hou, "Preparation of compact Al₂O₃ film on metal for oxidation resistance by polyvinylpyrrolidone," *J. Sol-Gel Sci. Technol.*, vol. 43, no. 3, pp. 321–327, May 2007.

- [139] B. H. H. Lohse, a. Calka, and D. Wexler, "Raman spectroscopy sheds new light on TiC formation during the controlled milling of titanium and carbon," *J. Alloys Compd.*, vol. 434–435, pp. 405–409, May 2007.
- [140] J. H. H. Lehman, M. Terrones, E. Mansfield, K. E. E. Hurst, and V. Meunier, "Evaluating the characteristics of multiwall carbon nanotubes," *Carbon N. Y.*, vol. 49, pp. 2581–2602, 2011.
- [141] V. Shanov, Y. Yun, and M. J. Schulz, "Synthesis and characterization of carbon nanotube materials (Review)," pp. 377–390, 2006.
- [142] D. A. Note, "Characterization of Carbon Nanotubes (CNTs) with Raman Spectroscopy," pp. 1–3.
- [143] M. Klein, J. Holy, and W. Williams, "Raman scattering induced by carbon vacancies in Ti C x," *Phys. Rev. B*, vol. 17, no. 4, pp. 1546–1556, Feb. 1978.
- [144] W. Kang, B. Cheng, Q. Li, X. Zhuang, and Y. Ren, "A new method for preparing alumina nanofibers by electrospinning technology," *Text. Res. J.*, vol. 81, no. 2, pp. 148–155, Sep. 2010.
- [145] M. Aghayan, I. Hussainova, M. Gasik, M. Kutuzov, and M. Friman, "Coupled thermal analysis of novel alumina nanofibers with ultrahigh aspect ratio," *Thermochim. Acta*, vol. 574, pp. 140–144, Dec. 2013.
- [146] S. Choi, S. Lee, C. Joo, S. Im, and S. Kim, "Formation of interfiber bonding in electrospun poly (etherimide) nanofiber web," *J. Mater. Sci.*, vol. 9, pp. 1511–1513, 2004.
- [147] G. W. Lee, "Phase Transition Characteristics of Flame-Synthesized Gamma-Al₂O₃ Nanoparticles with Heat Treatment," *Int. J. Chem. Nucl. Metall. Mater. Eng.*, vol. 7, no. 9, pp. 358–361, 2013.
- [148] S. Cava, S. M. Tebcherani, I. a. Souza, S. a. Pianaro, C. a. Paskocimas, E. Longo, and J. a. Varela, "Structural characterization of phase transition of Al₂O₃ nanopowders obtained by polymeric precursor method," *Mater. Chem. Phys.*, vol. 103, no. 2–3, pp. 394–399, Jun. 2007.
- [149] P. Figiel, M. Rozmus, and B. Smuk, "Properties of alumina ceramics obtained by conventional and non-conventional methods for sintering ceramics," *J. Achiev. ...*, vol. 48, no. 1, pp. 29–34, 2011.
- [150] S. H. Lee, C. Tekmen, and W. M. Sigmund, "Three-point bending of electrospun TiO₂ nanofibers," *Mater. Sci. Eng. A-Structural Mater. Prop. Microstruct. Process.*, vol. 398, pp. 77–81, 2005.
- [151] E. P. S. Tan and C. T. Lim, "Effects of annealing on the structural and mechanical properties of electrospun polymeric nanofibres.," *Nanotechnology*, vol. 17, no. 10, pp. 2649–54, May 2006.
- [152] L. Hu, H. Kim, J. Lee, P. Peumans, and Y. Cui, "Scalable coating and properties of transparent, flexible, silver nanowire electrodes," *ACS Nano*, vol. 4, no. 5, pp. 2955–63, May 2010.
- [153] B. Wu, A. Heidelberg, J. J. Boland, J. E. Sader, X. Sun, and Y. Li, "Microstructure-hardened silver nanowires," *Nano Lett.*, vol. 6, pp. 468–472, 2006.
- [154] D. R. Smith and F. R. Fickett, "Low-Temperature Properties of Silver," *J. Res. Natl. Inst. Stand. Technol.*, vol. 100, no. 2, p. 119, Mar. 1995.
- [155] S. Ogata, J. Li, N. Hirosaki, Y. Shibutani, and S. Yip, "Ideal shear strain of metals and ceramics," *Phys. Rev. B - Condens. Matter Mater. Phys.*, vol. 70, 2004.
- [156] H. Mao, J. Feng, X. Ma, C. Wu, and X. Zhao, "One-dimensional silver nanowires synthesized by self-seeding polyol process," *J. Nanoparticle Res.*, vol. 14, 2012.

PUBLICATIONS

CURRICULUM VITAE

Name: Madis Umalas
Date of birth: 25.09.1984
Phone: +372 53990865
E-mail: madis.umalas@ut.ee

Career:

2012–... University of Tartu, Institute of Physics, Specialist
2010–... Estonian Nanotechnology Competence Centre

Education:

2010–... University of Tartu, Faculty of Science and Technology,
Institute of Physics Materials Science Doctoral studies
2008–2010 University of Tartu, Faculty of Science and Technology,
Institute of Physics Materials Science Master's Degree
2004–2008 University of Tartu, Faculty of Science and Technology,
Institute of Physics Materials Science Bachelor's Degree
2004–2005 Compulsory military service
2001–2004 Pärnu Coeducational Gymnasium
1992–2001 Pärnu-Jaagupi High school

Research activity:

Application of sol-gel technology for production of ceramic nanocomposites and functional coatings

Honours & Awards:

2008, 2010, Madis Umalas; Honour at the stipend competition of Institute of Physics, University of Tartu

Dissertations supervised:

Kati Kongi, Master's Degree, 2014, (sup) Sven Lange, Madis Umalas, Optimization of stabilization conditions for electrospun polyacrylonitrile fibers, University of Tartu
Maarja Pohl, Bachelor's Degree 2014, (sup) Madis Umalas, Synthesis of titanium carbide and carbon nanotube composites by solgel technique, University of Tartu

Publications:

Umalas, M.; Hussainova, I.; Reedo, V.; Young, DL.; Cura, E.; Hannula, SP.; Lõhmus, R.; Lõhmus, A. (2015). Combined sol-gel and carbothermal synthesis of ZrC and TiC powders for composites. *Materials Chemistry and Physics*, vol. 153, pp. 301–306, Mar. 2015.

- Umalas, M.; Vlassov, S.; Polyakov, B.; Dorogin, L.; Saar, R.; Kink, I.; Lõhmus, R.; Lõhmus, A.; Romanov, A. (2014). Electron beam induced growth of silver nanowhiskers. *Journal of Crystal Growth*, 410, 63–68.
- Vlassov, S.; Polyakov, B.; Dorogin, L.; Antsov, M.; Mets, M.; Umalas, M.; Saar, R.; Lõhmus, R.; Kink, I. (2014). Elasticity and yield strength of pentagonal silver nanowires: In situ bending tests. *Materials Chemistry and Physics*, 134(3), 1026–1031.
- Umalas, M.; Reedo, V.; Lõhmus, A.; Hussainova, I.; Juhani, K. (2013). Synthesis of ZrC-TiC Blend by Novel Combination of Solgel Method and Carbothermal Reduction. Hussainova, I. (Eds.). *Engineering Materials and Tribology (62–67)*. Trans Tech Publications Ltd
- Umalas, M.; Reedo, V.; Lohmus, A.; Hussainova, I. (2012). Sol – gel solution based processing for nanocarbides. In: *Proceedings of the 8th International Conference od DAAAM Baltic Industrial Engineering 19–21st April 2012, Tallinn, Estonia: 8th International Conference of DAAAM Baltic Industrial Engineering, Tallinn, Estonia, 19–21 april 2012. (Eds.)* Otto, T.. Tallinn: Tallinna Tehnikaülikooli Kirjastus, 2012, 753–758.

Inventions

Invention: Use of Ionic Liquid as a Lubricant; Owner: University of Tartu; Authors: Raul Välbe, Jakob Kübarsepp, Rünno Lõhmus, Ants Lõhmus, Marta Tarkanovskaja, Valter Reedo, Madis Umalas, Uno Mäeorg; Priority number: UK1410837; Priority date: 18.06.2014

ELULOOKIRJELDUS

Nimi: Madis Umalas
Sünniaeg: 25.09.1984
Telefon: +372 53990865
E-mail: madis.umalas@ut.ee

Töökogemus:

2012– Tartu Ülikool, Loodus- ja tehnoloogiateaduskond,
Tartu Ülikooli Füüsika Instituut: spetsialist
2010– Eesti Nanotehnoloogiate Arenduskeskus AS

Haridus:

2010– Tartu Ülikool, Loodus- ja tehnoloogiateaduskond,
Doktoriõpe, Materjaliteadus
2008–2010 Tartu Ülikool, Loodus- ja tehnoloogiateaduskond,
Magistriõpe, Materjaliteadus
2004–2008 Tartu Ülikool, Loodus- ja tehnoloogiateaduskond,
Bakalaureuseõpe, Materjaliteadus
2004–2005
2001–2004 Pärnu Ühisgümnaasium
1992–2001 Pärnu-Jaagupi Keskkool

Teadustöö põhisuunad:

Keraamiliste nanokomposiitide ja funktsionaalsete pinnakatete sünteesi meetodi väljatöötamine sool-geel tehnoloogiaga ja nende karakteriseerimine erinevatel meetoditel.

Teaduspreemiad ja- tunnustused:

2008, 2010 Madis Umalas; Tunnustus Füüsika Instituudi üliõpilastööde konkursil

Juhendatud väitekirjad:

Kati Kongi, magistrikaad, 2014, (juh) Sven Lange, Madis Umalas, Polüakrüül-nitriilist elektrokedratud kiu stabiliseerimise režiimi optimeerimine, Tartu Ülikool
Maarja Pohl, bakalaureusekraad, 2014 (juh) Madis Umalas, Titaankarbiidi ja süsiniknanotorude komposiidi sünteesimeetodi väljatöötamine kasutades sool-geel tehnoloogiat, Tartu Ülikool

Publikatsioonid

Umalas, M.; Hussainova, I.; Reedo, V.; Young, DL.; Cura, E.; Hannula, SP.; Lõhmus, R.; Lõhmus, A. (2015). Combined sol-gel and carbothermal synthesis of ZrC and TiC powders for composites. Materials Chemistry and Physics, Mater. Chem. Phys., vol. 153, pp. 301–306, Mar. 2015.

- Umalas, M.; Vlassov, S.; Polyakov, B.; Dorogin, L.; Saar, R.; Kink, I.; Lõhmus, R.; Lõhmus, A.; Romanov, A. (2014). Electron beam induced growth of silver nanowhiskers. *Journal of Crystal Growth*, 410, 63–68.
- Vlassov, S.; Polyakov, B.; Dorogin, L.; Antsov, M.; Mets, M.; Umalas, M.; Saar, R.; Lõhmus, R.; Kink, I. (2014). Elasticity and yield strength of pentagonal silver nanowires: In situ bending tests. *Materials Chemistry and Physics*, 134(3), 1026–1031.
- Umalas, M.; Reedo, V.; Lõhmus, A.; Hussainova, I.; Juhani, K. (2013). Synthesis of ZrC-TiC Blend by Novel Combination of Solgel Method and Carbothermal Reduction. Hussainova, I. (Toim.). *Engineering Materials and Tribology (62–67)*. Trans Tech Publications Ltd
- Umalas, M.; Reedo, V.; Lohmus, A.; Hussainova, I. (2012). Sol – gel solution based processing for nanocarbides. In: *Proceedings of the 8th International Conference od DAAAM Baltic Industrial Engineering 19–21st April 2012, Tallinn, Estonia: 8th International Conference of DAAAM Baltic Industrial Engineering, Tallinn, Estonia, 19–21 april 2012. (Toim.) Otto, T.. Tallinn: Tallinna Tehnikaülikooli Kirjastus, 2012, 753–758.*

Patentsed leiutised

Patentne leiutis: Ioonvedeliku kasutamine määrdeainena; Omanik: Tartu Ülikool; Autorid: Raul Välbe, Jakob Kübarsepp, Rünno Lõhmus, Ants Lõhmus, Marta Tarkanovskaja, Valter Reedo, Madis Umalas, Uno Mäeorg; Prioriteedi-number: UK1410837; Prioriteedikuupäev: 18.06.2014

DISSERTATIONES SCIENTIAE MATERIALIS UNIVERSITATIS TARTUENSIS

1. **Martin Järvekülg.** Tubular microstructures by Hf-, Zr- and Ti-butoxide gel sheet rolling. Tartu, 2011, 112 p.
2. **Sergei Vlassov.** Investigation of nanoscale interactions and mechanical properties of nanostructures using quartz tuning fork based real-time measurements. Tartu, 2011, 171 p.
3. **Margus Kodu.** Pulsed Laser Deposition of Magnesium Oxide and Barium Ternary Oxides for Plasma Display Protective Layers. Tartu, 2011, 89 p.
4. **Rainer Pärna.** Surface studies of some oxide films. Tartu, 2011, 129 p.
5. **Jevgeni Šulga.** Self-assembly and interaction of nanostructures. Tartu, 2011, 114 p.
6. **Wojciech Kuznik.** Quantum-chemical computer simulations of the linear and non-linear optical properties of pyrazoloquinoline and dicyanopyrazine derivatives. Tartu, 2012, 89 p.
7. **Leonid Dorogin.** Structural and tribological properties of zero- and one-dimensional nanocrystals. Tartu, 2012, 193 p.
8. **Viljar Palmre.** Fabrication and characterization of microporous carbon-based electroactive polymer actuators. Tartu, 2012, 99 p.
9. **Madis Paalo.** Synthesis of CNT-metal oxide nanocomposites: sol-gel process, rheology, structural and functional properties. Tartu, 2014, 175 p.
10. **Raul Välbe.** Development of ionic liquid composites by sol-gel method for elaboration of industrial nano- and microstructures. Tartu, 2014, 97 p.
11. **Urmas Joost.** Impurity and preparation dependent properties of titania thin films. Tartu, 2014, 155 p.